Flavin-Mediated Chemotaxis near Poised Electrodes in *Shewanella oneidensis*

A THESIS
SUBMITTED TO THE FACULTY OF THE
UNIVERSITY OF MINNESOTA BY

Maria N. Lynch

IN PARTIAL FULFILLMENT OF THE REQUIREMENTS
FOR THE DEGREE OF
MASTER OF SCIENCE

Dr. Jeffery A. Gralnick

August 2025

ACKNOWLEDGEMENTS

First and foremost, I would like to thank my advisor, Jeff Gralnick. Jeff heard my career dreams from the get-go and gave me the academic freedom to pursue a research question that was of interest to me. He is a kind listener and a strong advocate, and I learned so much from him while discussing experimental design and interpreting results. I am grateful to be a part of the legendary Gralnick Lab.

I would also like to thank my *de facto* co-advisor, Daniel Bond. Daniel has a breadth of knowledge that never ceases to amaze me, and yet he always makes time to answer my questions, big or small. I am grateful for the opportunity to learn from him.

In addition to Jeff and Daniel, I would like to thank the third member of my thesis committee, Claudia Schmidt-Dannert. Thank you for reading my thesis and for allowing me to rotate in your lab. I not only learned integral cloning skills but also met wonderful friends.

Thank you to my lab mates who supported me, made me laugh, and taught me more than I could imagine: Maddie Ammend, Elena Ayala, Emily Hanson, Ursula Humayun, Vanita Indrakumar, Sophie Sanna, Parker Stoddard, and Mike Wold, as well as Drs. Brittany Bennett, Chi Ho Chan, David Hsu, Ivan Ishkov, Julian Schwanbeck, and Ruth Starwalt-Lee. Special thanks to Parker Stoddard, without whom I would not be in the Gralnick Lab, and the senior scientists who offered an expertise and mentorship that I did not know was possible.

Thank you to my Lynch family: Paul, Trudy, and Kyla. The dropped-off meals, restful nights at Edgewater, and interest in my work have brought so much joy to my studies. Thank you for supporting me and always asking me about my research!

Thank you to my Kisch siblings Karli, Michael, and Kaity for early morning coffees, late night 3D printing, and the knowledge that you always have my back.

Thank you to my parents, Chris and Cathy Kisch. You fostered early dreams of marine biology, cheered me on during organic chemistry, and now have walked with me during my MicE degree. Your encouragement has been with me every step of the way. Thank you.

Finally, I would like to thank my husband, Ethan. You are the partner of my heart, and it is a privilege to be married to you.

May the Lord bless you and keep you.
May He make His face shine on you and be gracious to you.
May He turn His face toward you and give you peace.
Numbers 6:24-26

DEDICATION

To my mom, Cathy Kisch. Your unwavering support means the world to me.

ABSTRACT

Shewanella oneidensis is a facultative anaerobe renowned for its ability to perform extracellular electron transfer, a process mediated by direct contact with electron acceptors or by released flavins such as riboflavin and flavin mononucleotide. These flavins enable *S. oneidensis* to adapt to dynamic environments and also act as chemoattractants, potentially influencing motility toward insoluble electron acceptors such as electrodes. While flavins are known chemoattractants, the role of their redox state in influencing bacterial behavior remains unclear. This work hypothesizes that *S. oneidensis* exhibits enhanced chemotaxis toward oxidized flavins. Because flavins are oxidized upon interacting with environmental electron acceptors, detecting and moving up gradients of oxidized flavins may help the bacterium locate insoluble electron acceptors beneficial for its survival. To test our hypothesis that oxidized flavins are specifically recognized by *S. oneidensis*, we developed a novel experimental platform combining high-resolution microscopy, electrochemical analysis, and Python-based motility quantification. A glass microscope slide patterned with indium tin oxide regions was used for experiments, and its design allowed electrochemical control of flavin redox states using a potentiostat. The setup generated localized redox gradients and enabled real-time visualization of bacterial motility under anaerobic conditions. Results indicate that *S. oneidensis* electrolocates to the poised electrode, which is rich in oxidized flavins compared to reduced flavins. In contrast, a mutant deficient in chemotaxis sensing (*S. oneidensis* Δ*cheA-3*), did not demonstrate electrolocation behavior. Mutants deficient in extracellular electron transport also lacked an electrolocation phenotype, but the analysis was limited due to experimental factors. These findings advance our understanding of flavins as both electron shuttles and chemoattractants and set the stage to further investigate the mechanism of redox sensing in the genus *Shewanella*.

Supplementary information attached to this work includes videos and Python code used to analyze cell congregation data. Movie 1 depicts the formation of a flavin gradient; Movie 2 depicts wild-type *S. oneidensis* MR-1, with the poised electrode on the right; Movie 3 depicts wild-type *S. oneidensis* MR-1, with the poised electrode on the left; Movie 4 depicts *S. oneidensis* Δ*cheA-3* with the poised electrode on the right; Movie 5 depicts *S. oneidensis* Δ*cheA-3* with the poised electrode on the left. Movie 6 depicts *S. oneidensis* lacking cytochromes necessary for EET (*S. oneidensis* ΔEET), with the poised electrode on the right; Movie 7 depicts *S. oneidensis* lacking cytochromes necessary for EET (*S. oneidensis* ΔEET), with the poised electrode on the left. See Table A for full movie descriptions. Finally, the file 20250827_Video_Analysis_Code contains the code used to analyze cell density data and create the graphs.

TABLE OF CONTENTS

LIST OF TABLES

LIST OF FIGURES

CHAPTER 1:
INTRODUCTION TO THE WORK

Perspective

From the development of beer and cheese made possible by microbial fermentation, to the use of nitrogen-fixing bacteria *Bradyrhizobia* in regenerative agriculture, microbes have the power to inspire solutions to the issues that face human society. As we continue to deepen our knowledge of the metabolisms, mechanisms, and survival strategies of earth's earliest life form (Vinnichenko *et al.*, 2020), biologists are poised to be heralds of the evolutionary genius that microbes contain (Snell-Rood, 2016). Fundamental microbiological research can drive technologies that transform industries, promote sustainability, and inspire new engineering approaches. One microorganism that has been leading inspiration since its discovery is *Shewanella oneidensis*.

S. oneidensis is of particular interest to the bio-inspired design community due to its unique respiratory versatility. Cellular respiration converts molecular energy into energy a cell can use, typically by oxidizing a molecule in the cytoplasm and channeling the resulting electrons through a membrane-embedded electron transport chain. For aerobic respiration, oxygen serves as the terminal electron acceptor that drives proton translocation and consequent ATP synthesis. For anaerobic respiration, the cell uses alternative electron acceptors such as nitrate or sulfate to drive energy production.

Many organisms specialize in either aerobic or anaerobic respiration, but facultative anaerobes like *S. oneidensis* can switch between modalities depending on environmental conditions. *S. oneidensis* is particularly remarkable as a facultative anaerobe, because it can respire using over 20 terminal electron acceptors, displaying a respiratory versatility that is unmatched by another known organism ("Ecophysiology of the Genus Shewanella," 2006; Hau & Gralnick, 2007). This extraordinary respiratory capacity is dependent on extracellular electron transport (EET). The proteins that comprise the EET pathway allow for respiration using substrates that range from soluble acceptors such as fumarate and nitrate to insoluble acceptors such as manganese oxides and iron oxides (Murphy & Saltikov, 2007; Myers & Nealson, 1990; Schwalb *et al.*, 2002). Notably, EET also enables *S. oneidensis* to transfer electrons to the solid surface of a poised electrode (Gorby *et al.*, 2006; Hau & Gralnick, 2007), generating current (Bretschger *et al.*, 2007). Thus, *S. oneidensis* serves as a model organism for EET and its applications in microbial fuel cells, bioremediation, and mineral cycling in the environment (Kappler *et al.*, 2021; Marshall *et al.*, 2006; Nealson, 2017).

Using the proteins of the EET pathway to respire both soluble and insoluble substrates is critical for shewanellae survival in diverse ecological niches (Hau & Gralnick, 2007). Despite significant advances in understanding the components of *Shewanella* EET, a key question remains: How does *S. oneidensis* locate and move toward insoluble electron acceptors in its environment? The ability of *S. oneidensis* to navigate toward insoluble substrates is essential for utilizing them as terminal electron acceptors, and yet the mechanisms underlying this ability are not well understood. This thesis investigates the hypothesis that *S. oneidensis* secretes its own navigation system in the form of flavins, and it uses a gradient of oxidized flavins to locate and swim toward insoluble electron acceptors. By exploring the navigation mechanisms of *S. oneidensis* toward the electrode, this study aims to prove that oxidized flavins are the chemoattractant utilized by the cells to detect the presence of an insoluble electron acceptor (IEA).

Ecological niche of *Shewanella oneidensis*

Shewanella oneidensis was one of the first dissimilatory metal-reducing bacteria to be recorded in the literature (Myers & Nealson, 1988). It was enriched from the sediment of Oneida Lake in New York, and it was originally called *Alteromonas putrefaciens* MR-1. However, it was later renamed *Shewanella putrefaciens* MR-1 (MacDonell & Colwell, 1985) before the final name of *Shewanella oneidensis* MR-1 was selected (Venkateswaran *et al.*, 1999). The name *Shewanella oneidensis* MR-1 reflects the lake of its isolation (Myers & Nealson, 1988), the taxonomy that sequencing revealed (Venkateswaran *et al.*, 1999), and its ability to perform manganese reduction (MR-1).

The sediment where *S. oneidensis* MR-1 was first isolated constitutes a dynamic environment. It is aerobic at the sediment-water interface and anerobic just a few millimeters below the sediment surface (Myers & Nealson, 1988). The environment also has a dynamic flux of nutrients in addition to varying electron acceptors and donors, a common trait of the ecological niche that shewanellae tend to occupy ("Ecophysiology of the Genus Shewanella," 2006; Hau & Gralnick, 2007). Though shewanellae preferentially use oxygen as a high-energy electron acceptor in its environment, living in a rapidly changing environment demands the ability to be metabolically diverse (Fredrickson *et al.*, 2008). When oxygen or another soluble electron acceptor is unavailable, *S. oneidensis* uses EET to reduce insoluble substrates beyond its cell membrane. It transports electrons to anaerobic oxidants in two primary ways: through direct contact between extracellular proteins and the insoluble electron acceptor itself, and through the

mediation of redox-active shuttles (Brutinel & Gralnick, 2012; Gralnick & Newman, 2007). The mechanisms of EET via direct contact and via shuttles are particularly relevant to this work.

Extracellular Electron Transport

Electron Transfer via Direct Contact

EET is useful to the cell when an oxidant cannot diffuse across the cell membrane or would cause harm if it did, as is the case for shewanellae growing in soils contaminated with chromium, where the soluble form of Cr(VI) is reduced by *S. oneidensis* to its less toxic form of Cr(III) (Wang *et al.*, 2014). The process of EET is performed through a series of metal respiratory system (Mtr) proteins (Coursolle & Gralnick, 2010) that are primarily *c*-type cytochromes (Shi *et al.*, 2007). The Mtr proteins have a hierarchy of functions. For example, MtrA, MtrB, and MtrC play the primary roles in EET, but homologous proteins in *S. oneidensis* such as MtrD, MtrE, and MtrF offer partial compensation in EET if a primary player is lost. Since MtrC and its paralogue OmcA play a major role in reducing electrodes and flavins, the proteins originating from the *omcA-mtrCAB* gene cluster will be discussed in detail (Clarke *et al.*, 2011; Coursolle *et al.*, 2010) (Figure 1A).

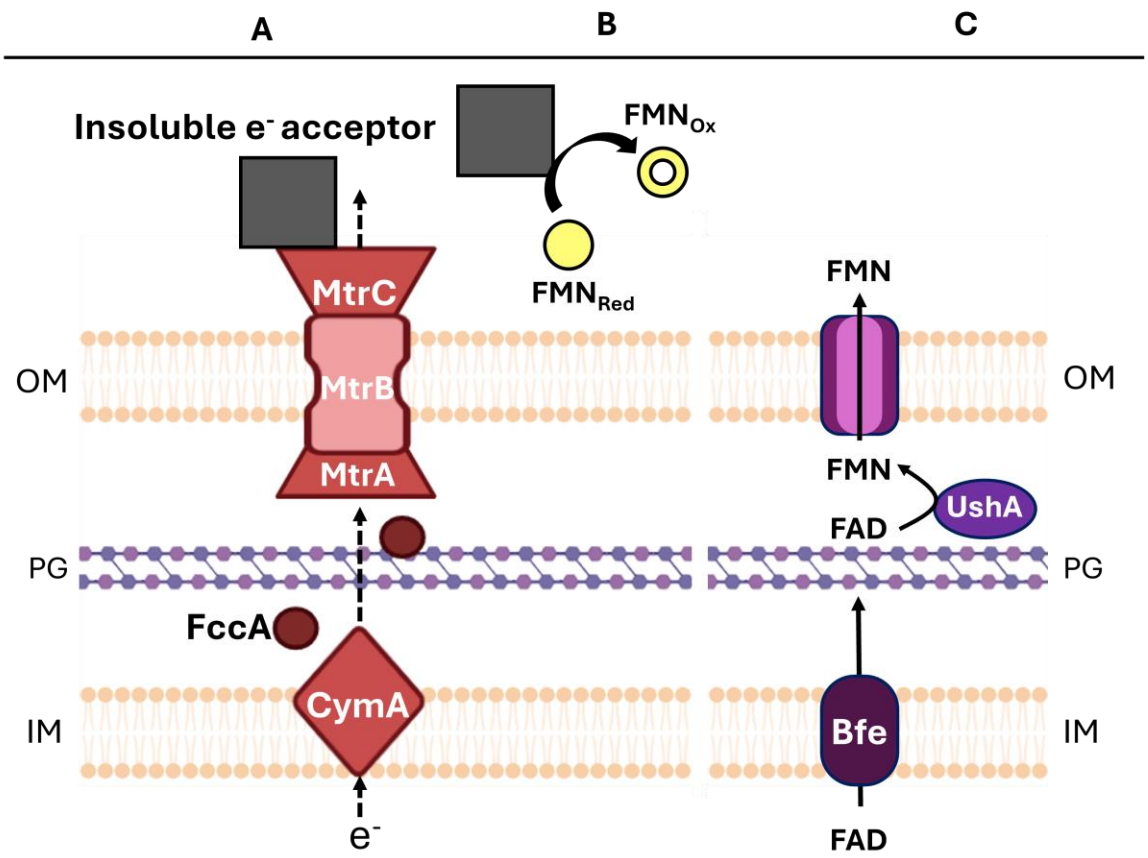

Figure 1: *S. oneidensis* uses direct and indirect methods to reduce insoluble electron acceptors via EET. The figure is divided into three sections. The first section **(A)** depicts the flow of electrons (dashed lines) through the proteins involved in EET to reduce an IEA by direct contact. The second section **(B)** represents the use of reduced flavin mononucleotide (FMN_{Red}) to reduce an IEA indirectly, with FMN becoming oxidized in the process (FMN_{Ox}). The third section **(C)** describes the secretion of flavin adenine dinucleotide (FAD) into the periplasm, where it is cleaved to FMN and diffuses out of the cell to be utilized as a redox-active shuttle.

First, CymA accepts electrons from the menaquinone pool in the inner membrane (Gralnick & Newman, 2007; Myers & Myers, 1997). CymA is a tetraheme *c*-type cytochrome that is integral for all anaerobic respiration in *Shewanella*, except when respiring thiosulfate and trimethylamine *N*-oxide (TMAO) as terminal electron acceptors (Saffarini *et al.*, 2002). CymA then transfers electrons to the periplasmic proteins FccA or CctA (Fonseca *et al.*, 2013). Though FccA is a fumarate reductase and CctA has specific functions related to the nitrate reductase, both proteins serve the overlapping role of ferrying electrons through the periplasmic space to the

outer membrane (OM) (Pitts *et al.*, 2003; Schuetz *et al.*, 2009; Schwalb *et al.*, 2002). FccA or CctA transfers electrons to MtrA, a decaheme *c*-type cytochrome (Pitts *et al.*, 2003). MtrA is partially embedded in the β-barrel porin MtrB, which forms a conductive channel allowing electrons to flow through the hemes of MtrA and reach the terminal reductase located on the outside of the cell (Edwards *et al.*, 2020; Hartshorne *et al.*, 2009; Pitts *et al.*, 2003). The terminal reductase MtrC directly interacts with an insoluble electron acceptor like an electrode (Coursolle & Gralnick, 2010; Shi *et al.*, 2007).

Electron Transfer Mediated by Flavins

The second method by which shewanellae reduce insoluble electron acceptors relies on electron shuttles (Figure 1B). In particular, outer membrane cytochromes MtrC and OmcA contain heme groups that interact with flavins (Paquete *et al.*, 2014), which are redox-active small molecules known to be electron shuttles (Marsili *et al.*, 2008). Flavins are made in the *S. oneidensis* periplasm as flavin adenine dinucleotide (FAD) (Figure 1C). A protein in the family of multidrug and toxin efflux pumps, Bfe, exports FAD into the periplasm (Kotloski & Gralnick, 2013). Once in the periplasm, the 5' nucleotidase UshA hydrolyses FAD into flavin mononucleotide (FMN) and adenosine monophosphate (AMP) (Covington *et al.*, 2010). The FMN then diffuses out of the cell through outer membrane porins (Covington *et al.*, 2010). It either leaves the cell in its reduced state, or it is reduced by MrtC and diffuses into the surrounding environment (Coursolle *et al.*, 2010). Thus, when the flavin encounters a suitable electron acceptor in the environment, it donates its electrons and becomes re-oxidized. By cycling between oxidized and reduced forms, FMN can act as a reversible, diffusible mediator that shuttles electrons between the cell's OM cytochromes and more distant oxidants.

Numerous *Shewanella* species produce flavins that result in FMN accumulating in their surroundings (von Canstein *et al.*, 2008). FMN benefits the cells not only by increasing the range at which they can reduce oxidants, but also by influencing the organism's current-producing capacity. The presence of flavins increases the rate of electron transfer by over four-fold compared to conditions without flavins (Marsili *et al.*, 2008). Additionally, FMN exhibits a midpoint potential around −0.2 V vs. a standard hydrogen electrode (SHE), enabling cells to reduce electrodes at potentials that are relative to flavins as well as the EET proteins involved in direct transfer mechanisms (Baron *et al.*, 2009; Okamoto *et al.*, 2014). It is estimated that flavin-mediated EET accounts for ~75% of a cell's ability to respire using insoluble electron acceptors (Brutinel & Gralnick, 2012; Kotloski & Gralnick, 2013). Therefore, flavins contribute

significantly to the ability of shewanellae to survive in environments with rapid redox changes and the need to respire using diverse substrates.

Though flavins aid the ability of *S. oneidensis* to reduce oxidants at a distance, the secretion of flavins is present even in strains incapable of performing EET (Coursolle *et al.*, 2010). Furthermore, flavins are secreted when *S. oneidensis* is grown both aerobically and anaerobically (Kees *et al.*, 2019; von Canstein *et al.*, 2008), raising questions about why cells would make and secrete flavins when not directly utilizing them. The consistency of flavin secretion in the *Shewanella* growth strategy suggests that flavins serve more than one physiological purpose for the cell.

Chemotaxis

Recent studies have probed the idea that flavins can act as a chemoattractant for shewanellae, lending insight into how *S. oneidensis* might use chemotaxis to navigate toward insoluble electron acceptors (R. Li *et al.*, 2012). Chemotaxis is the biased, random walk a motile cell takes along chemical gradients in its environment (Berg, 1975). *S. oneidensis* is motile due to a single flagellum located at its pole (Venkateswaran *et al.*, 1999). The fibers of the flagellum extend from the cell body and rotate in a helical fashion to move cells up or down a chemical gradient (Berg & Anderson, 1973). The rotation of the flagellum is powered by the movement of protons or sodium ions across the cell's inner membrane. The use of proton motive force generated from respiration to power motility directly links the cell's ability to swim to its energy state. The flagellum complex has three main parts: the basal body, the flagellar hook, and the filament (Thormann *et al.*, 2022) (Figure 2). The basal body's position is optimal for interacting with both intercellular and extracellular proteins that produce motility.

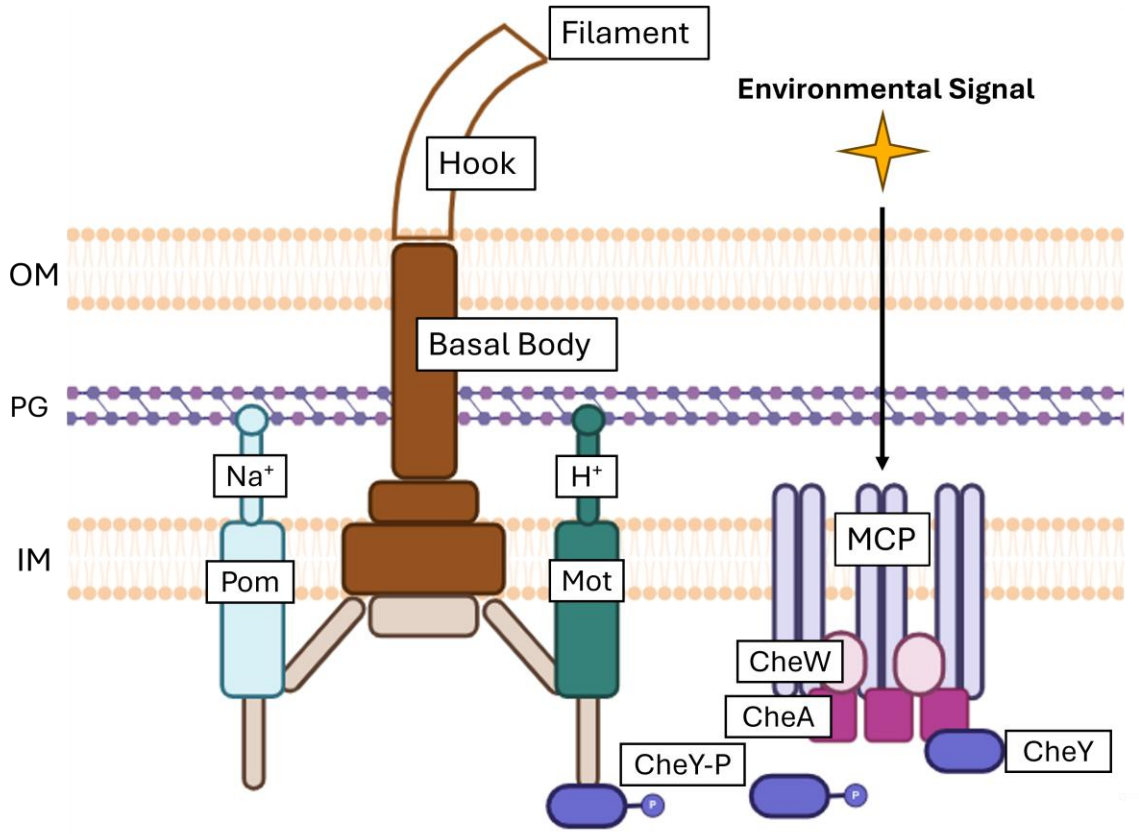

Figure 2: *S. oneidensis* utilizes chemotaxis proteins to sense and respond to chemical gradients in its environment. An environmental signal diffuses across the outer membrane and interacts with an array of methyl-accepting chemotaxis proteins (MCPs) in the inner membrane. The MCPs are aggregated by CheW, and the signal is transduced through the CheA protein which phosphorylates CheY. Phosphorylated Chey (CheY-P) binds to the motor proteins (Mot) which triggers a change in direction of flagellar rotation. The flagellar rotation can be driven by a proton (H^+) pump or a sodium ion (Na^+) pump.

As *Shewanella* species are often found in diverse environments with rapidly changing concentrations of nutrients, they are ideal organisms for a "gradient lifestyle" ("Ecophysiology of the Genus Shewanella," 2006). A gradient lifestyle provides a plausible reason for the large amount of chemotaxis genes found within the *Shewanella* genome that would increase the cell's fitness in navigating toward beneficial substrates (J. Li *et al.*, 2007; Starwalt-Lee *et al.*, 2021). For example, methyl-accepting chemotaxis proteins (MCPs) are essential for chemotaxis. Where *E. coli* contains 5 MCP complexes, *S. oneidensis* contains at least 26 MCPs, indicating a potentially high importance of navigation machinery in *S. oneidensis* (Heidelberg *et al.*, 2002;

Starwalt-Lee *et al.*, 2021). Through a dedicated system of chemotaxis (Che) proteins that work together with the MCPs, the chemical signal is received by the cell and induces movement up a gradient toward favorable conditions or down a gradient away from harmful conditions (Keegstra *et al.*, 2022).

The MCPs are embedded in the inner membrane and form the core of a two-component signal-transduction pathway (Hazelbauer *et al.*, 1990). MCPs can sense chemical gradients in two ways: by directly binding a chemical to an associated ligand, or by sensing shifts in the cell's proton motive force that result from substrate interactions. The latter method is called energy taxis (Baraquet *et al.*, 2009). Energy taxis aids the cell in navigation toward compounds that alter its energy status, not only influencing the cell's metabolic functioning but also affecting the energy available for powering flagellar rotation.

When the MCP transduces a signal, the scaffolding protein CheW triggers the autophosphorylation event of the histidine kinase CheA. CheA can then transfer its phosphate group to the response regulator, CheY, and phosphorylated CheY binds directly with the motor proteins of the flagellar basal body. When CheY is bound to the basal body proteins, it causes a change in the rotation of the flagellum that reverses the cell's direction (J. Li *et al.*, 2007) (Figure 2). The higher the concentration of a substrate, the more often the MCP transduces a signal, and the more often flagellar rotation changes.

When the direction of the flagellar rotation changes, *S. oneidensis* changes its motility pattern. Its motility pattern consists of forward runs, reversals, and a "reverse and flick" motion that results in reorientation (Stocker, 2011; Thormann *et al.*, 2022). In addition to the previously described motility patterns, *S. oneidensis* can transition between fast, longitudinal swimming and slower, sideways swimming which are characteristic of mono- and multiflagellate bacteria, respectively (Stricker *et al.*, 2020). The ability to switch swimming strategies may increase the cell's ability to compete across diverse ecological niches (Stricker *et al.*, 2020). A higher gradient of a chemical leads to shorter runs and a more localized area of swimming.

There is evidence of shewanellae chemotaxis to many compounds, including but not limited to nitrate, nitrite, dimethyl sulfoxide (DMSO), anthraquinone-2,6-disulfonate (AQDS), TMAO, soluble Fe(II), and soluble Mn(II) (Bencharit & Ward, 2005; Nealson *et al.*, 1995). *S. oneidensis* even displays chemotaxis toward insoluble electron acceptors in anaerobic environments (Harris *et al.*, 2010). Chemotaxis in relation to insoluble electron acceptors is unique, because insoluble substrates such as the electrode are often separated from the cell by distance, are themselves immobile, and produce no gradient detectable by inner membrane

proteins, as is thought to be necessary for chemotaxis. Even though insoluble acceptors such as manganese oxide or electrodes do not emit a detectable gradient, *S. oneidensis* still exhibits the hallmarks of chemotaxis within a radius of its redox-active surface: cell reversal frequencies increase and cell swim speeds increase. This unusual behavior near IEAs was first termed "electrokinesis" by Harris *et al.* (2010) and was later expanded to include congregation at the redox-active surface (Harris *et al.*, 2012). Starwalt-Lee *et al.* (2021) then introduced the term "electrolocation" to describe the process by which cells may sense and navigate toward IEAs in their environment. Since electrolocation encompasses both the motility responses and the sensory mechanisms potentially underlying the behavior, it will be adopted throughout this work. Electrolocation represents a unique intersection of chemotaxis and extracellular electron transport (EET) and serves as the conceptual framework for the studies presented here.

Components of Electrolocation

As studies have explored the peculiarities of electrolocation, three primary principles have become apparent. First, electrolocation requires functional EET. When observing *S. oneidensis* strains deficient in EET (Δ*mtrA*, Δ*mtrB*, and Δ*cymA*, respectively) near an anaerobic electron acceptor, no change in swimming speed is observed, and cells do not increase their reversal frequencies near the particulate (Harris *et al.*, 2010). As a result, cells are unable to congregate around the mineral, and the absence of congregation is an indication that cells are unable to navigate toward the redox-active surface (Harris *et al.*, 2012).

Further evidence supporting the link between electrolocation and EET is provided by comparative studies of *Shewanella* strains. Experiments reveal that the electrokinetic response to manganese oxide varies in strength according to the species' current-generating capacity. For instance, *S. oneidensis* MR-1 can generate the most current and exhibits the strongest electrokinetic response, whereas *S. putrefaciens* CN32 can generate the least current and exhibits the weakest electrokinetic response (Harris *et al.*, 2010). The correlation between current generation and electrokinetic response suggests that electrokinesis is related to electron flow and may also influence energy taxis due to changes in the cell's proton motive force.

A second principle of electrolocation that builds on the requirement of EET is that *S. oneidensis* cells exhibit an electrolocation phenotype in relation to changing redox potential. *S. oneidensis* cells swim faster near electrodes that are poised at a more positive potential (Harris *et al.*, 2010). For example, an electrode poised at 0.3 V vs. SHE induced faster swimming speeds than an electrode poised at −0.3 V vs. SHE (Oram & Jeuken, 2019). Furthermore, the tactic shift

for increased swim speeds and reversal frequencies occurs within a potential range that coincides with the midpoint potential of flavins: between −0.25 and −0.15 V vs. SHE (Oram & Jueken, 2019). Deleting both *mtrC* and *omcA* to disrupt the EET pathway greatly decreased the tactic shift (Oram & Jueken, 2019). Thus, EET is necessary for cells to not only sense the presence of the electrode but also to sense the potential at which the electrode is poised.

The third principle known about electrolocation is that it depends upon a functional chemotaxis system. When investigating a mutant deficient in the chemotaxis gene *cheA-3*, studies observe only a partial phenotype: cells increase their swim speed near the electrode, but they do not change direction of their runs. As a result, *cheA-3* deletion mutants do not congregate near the electrode and are unable to navigate toward it (Harris *et al.*, 2012).

Flavins as Mediators of Electrolocation

Studies have suggested that due to the need for EET, the tactic switch that is observable at the midpoint potential of flavins, and the dependence on chemotaxis for congregation, *S. oneidensis* uses flavins to navigate toward insoluble electron acceptors (R. Li *et al.*, 2012); Oram & Jueken, 2019). The hypothesis would indicate that as cells excrete flavins into the environment, the flavins are excreted in a reduced state or are actively reduced by MtrC. As the reduced flavins diffuse away from the cell and encounter an oxidant, the flavins become oxidized. Therefore, a gradient of reduced to oxidized flavins forms, with the reduced flavins being nearest to the cell, and the oxidized flavins being nearest to the oxidant (R. Li *et al.*, 2012). By sensing the presence of oxidized flavins through its MCPs, the cell could navigate toward an insoluble electron acceptor such as manganese, because there would be a higher concentration of oxidized flavins in its vicinity. It is known that flavins are indeed a chemoattractant for shewanellae (Kim *et al.*, 2016; R. Li *et al.*, 2012) and that the addition of flavins enhances the chemotactic response to anaerobic electron acceptors (Harris *et al.*, 2010; Y. Li *et al.*, 2022; Oram & Jeuken, 2019). Yet, it remains unclear if oxidized flavins form the extracellular gradient required for shewanellae to locate insoluble substrates. To fill the existing knowledge gap, I will employ electrochemistry, microscopy, and computer programming techniques to test whether *S. oneidensis* exploits oxidized-flavin gradients as its navigational signal to reach insoluble electron acceptors.

CHAPTER 2:
EXPERIMENTAL METHODS

Overview

To test the hypothesis that oxidized flavins act as chemoattractants and facilitate shewanellae navigation toward insoluble electron acceptors, four core components were needed: bacterial strains relevant to the study, an anaerobic microscope for live-cell imaging and recording, a system to precisely control electrochemical parameters, and software to analyze bacterial movement.

Bacterial Strains and Cell Preparation

Strain Details

Three strains were utilized for experimentation: *S. oneidensis* strain MR-1, *S. oneidensis* lacking the essential chemotaxis gene *cheA-3* (Δ*cheA-3*), and *S. oneidensis* lacking cytochromes that comprise the EET pathway: *S. oneidensis* Δ*mtrCAB*, Δ*omcA*, Δ*mtrDEF*, Δ*dmsE*, ΔSO4360, Δ*cctA*, Δ*fccA*, and Δ*cymA*, hereafter referred to as the ΔEET strain. *S. oneidensis* MR-1 was originally isolated from Lake Oneida in New York, USA (Myers 1988) and is identified as JG274 in the Gralnick strain collection. *S. oneidensis* Δ*cheA-3* (ΔSO_3207) was made by Ruth Starwalt-Lee and is identified as JG4863 in the Gralnick strain collection. The ΔEET strain was made by Bridget Conley (unpublished) and is identified as JG3893 in the Gralnick strain collection.

The in-frame deletion of *cheA-3* was generated using methods adapted from Saltikov & Newman (2003). In brief, fragments 1 kb upstream and downstream of *cheA-3* were made using primers indicated in Table 1. The primers were designed to include flanking SpeI and SacI restriction enzyme sites, respectively. The upstream and downstream fragments were fused together and ligated into the suicide vector pSMV3, which carries a kanamycin resistance and a *sacB* cassette (Kees *et al.*, 2019; Saltikov & Newman, 2003). The resulting pSMV3$^{\Delta cheA\text{-}3}$ plasmid was transformed into *E. coli* UQ950 for plasmid replication and storage (Saltikov & Newman, 2003). The plasmid was extracted from the cell and sequenced using M13 primers to ensure accuracy for downstream usage. Once the plasmid's sequence was confirmed, the plasmid was introduced into electrocompetent *S. oneidensis* via electroporation. Merodiploids containing a single crossover event were selected for on lysogeny broth (LB) plates containing 50 µg/mL kanamycin. Strains that integrated the plasmid were counter selected for on LB plates containing 10% sucrose. PCR confirmed the loss of the *cheA-3* from the *S. oneidensis* genome, and the strains were sequenced for accuracy.

Table 1: Primers used to make in-frame deletion of *cheA-3* from the *S. oneidensis* genome.

Primer Description	Restriction Enzyme	Primer Sequence 5' to 3'
Upstream Forward	SpeI	ACGACTAGTCATGCAGGGTATCGATTTGCTTAAGGC
Upstream Reverse	N/A	CCATTCCATTCCTTAACTTGGAAACTAACTATCAAAGGCCATCAAATTGACTCCCAG
Downstream Forward	N/A	CTGGGAGTCAATTTGATGGCCTTTGATAGTTAGTTTCCAAGTTAAGGAATGGAATGG
Downstream Reverse	SacI	ACGGAGCTCCCATAGACGACACAACTCGCTTCAT

Growth Conditions and Preparation for Experiments

From -80°C glycerol stocks, cells were streaked onto a LB plate and allowed to incubate at 30°C overnight. A single colony was then used to inoculate 2 mL of liquid LB. The LB culture was incubated 15-22 hours at 30°C while shaking at 250 RPM. The overnight culture was then diluted to an optical density at 600 nm (OD_{600}) of 0.1 in fresh LB. It was incubated at 30°C while shaking at 250 RPM until the cells were in exponential growth phase, at an OD_{600} between 0.6 and 1.0, depending on the experiment.

Once sufficient cell density was attained, the LB culture was diluted into a modified recipe of anaerobic *Shewanella* Basal Medium (SBM) (Hau *et al.*, 2008) for use in microscopy (SBM-M1). Per liter, SBM-M1 contained 0.225 g K_2HPO_4, 0.225 g KH_2PO_4, 0.46 g NaCl, 0.225 g $(NH_4)_2SO_4$, and 0.117 g $MgSO_4 \cdot 7H_2O$. It also contained 20 mM sodium D,L-lactate as electron donor, 40 mM sodium fumarate as electron acceptor, and 100 mM HEPES buffer. The final pH was adjusted to 7.2. Vitamins, amino acids, and minerals were excluded from media preparation to decrease the abundance of alternative chemoattractants present in the media.

After being diluted in anaerobic SBM-M1, the culture was incubated in the anaerobic chamber (Coy Laboratory Products, Inc; Grass Lake, MI, USA) for 2-3 hours at room temperature. Motility was checked by microscopy before continuing with the experiment. Once sufficient motility was established, the culture was then further diluted in a solution containing flavins, using gentle flicks to mix the solution to avoid shearing the flagella. The flavin stock solution was 10 mM FMN suspended in SBM salts (per liter: 0.225 g K_2HPO_4, 0.225 g KH_2PO_4,

0.46 g NaCl, 0.225 g $(NH_4)_2SO_4$, and 0.117 g $MgSO_47H_2O$) with 100 mM HEPES. The solution was purged with argon gas then filter sterilized into an anaerobic, sterile Balch tube. It was shielded from light and stored at 4°C to prevent photodegradation (Marsili *et al.*, 2008).

Across all experiments, dilutions were performed so that the final OD_{600} for microscopy was estimated to be between 0.03 and 0.09. Also in the final microscopy sample, the final concentration of fumarate was estimated to be between 1.3 mM and 2.0 mM, the lactate concentration was estimated to be between 0.6 mM and 2.5 mM, and the FMN concentration was estimated to be between 7.5 mM and 9.0 mM. Concentrations varied across the experimental treatments, but all concentrations remained in the millimolar range. Future experiments will optimize component concentrations and maintain consistency across treatments.

Experimental Setup

Anaerobic Environment

An anaerobic environment was established using a vinyl anaerobic chamber (Coy Laboratory Products, Inc; Grass Lake, MI, USA). The atmosphere contained 5% H_2 with the balance as N_2. The anaerobic chamber was modified with a plug to allow electrical cables to enter the chamber while maintaining the anaerobic environment.

Imaging System

Cells were visualized using a microscope placed within the anaerobic chamber (Revolve Microscope, Discover Echo; San Diego, CA, USA). An iPad attached to the microscope allowed photo and video recordings of cell motility through the iPad camera. For the videos discussed in this work, recordings were taken using a 20-x objective under phase contrast.

Specialized microscope slides were obtained from collaborator Mohamed El-Naggar from the University of Southern California (Figure 3). In brief, the glass slides (3.25 cm^2) were modified to have two rectangular electrodes (1.25 x 0.5 cm^2) made of indium tin oxide (ITO) deposited onto the slide surface separated by a 200 μm gap. ITO is a redox-active and transparent material which allows for control of the electrode potential as well as visualization of cells swimming over its surface. Before use in experiments, the glass slides were washed for 30 seconds in acetone, isopropyl alcohol, ethanol, and deionized water, respectively. The washing steps were performed to remove the photoresist in which the slides were packaged (Cristina Niman, personal communication), decrease bacterial adhesion to the glass, and clean the glass for optical optimization (R. Li *et al.*, 2012) (Stricker *et al.*, 2020). The slides were then dried with

blotting paper or lens paper, and ITO conductivity was confirmed using a multimeter. An 18 mm^2, number 1.5 coverslip (Thermo Fisher Scientific, Inc; Waltham, MA, USA) was used with the microscope slide.

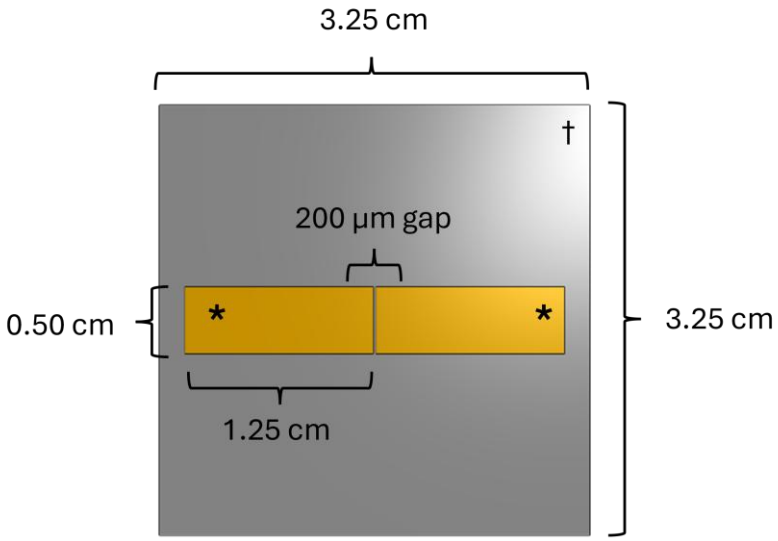

Figure 3: The custom ITO-patterned glass microscope slide used for experiments. The rendered image displays the dimensions of the glass slide **(†)** and denotes the redox-active surface of the ITO electrodes **(*)**. The electrodes are separated by a 200 µm gap.

Electrochemical Setup

A custom microscope stage held the glass slide in place for imaging and served to facilitate the electrochemical connections. The stage was designed in collaboration with Ivan Ishkov using OnShape and 3D printed using polylactic acid (PLA) (Figure 4). In brief, the microscope stage held the coverslip securely in place and ensured contact between the wire leads and ITO electrode surface. The wires were then connected via alligator clips to the potentiostat (AFCBP1-23364821; Pine Instrument Company; Grove City, PA, USA) leads located inside the anaerobic chamber. The potentiostat itself was located outside of the anaerobic chamber.

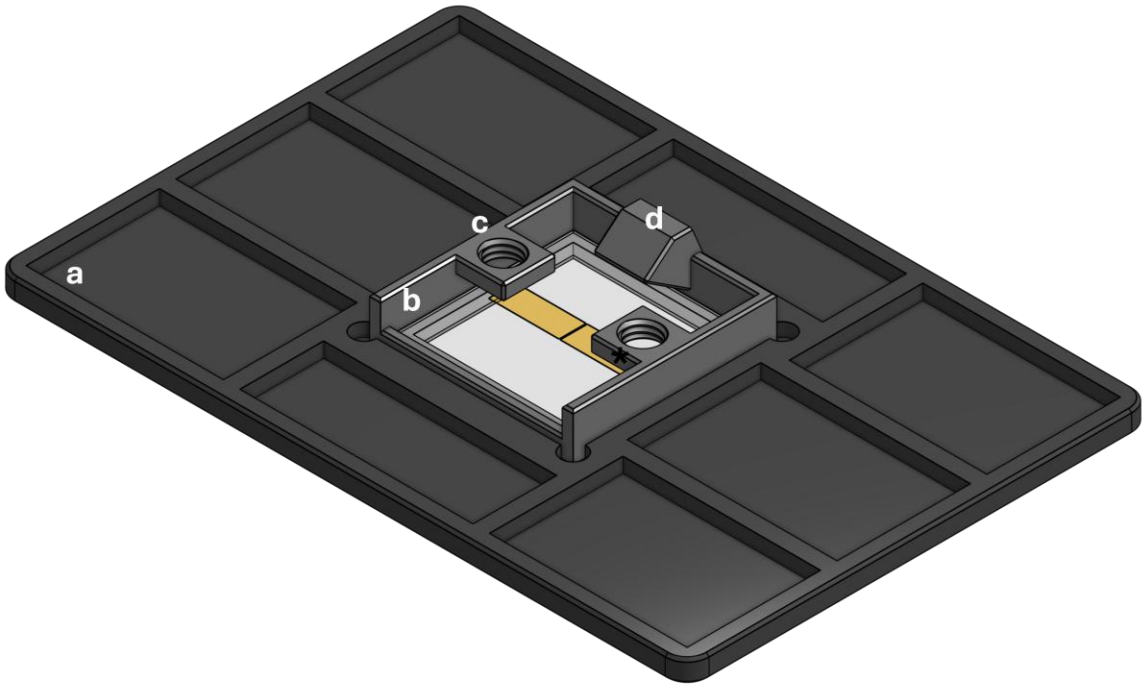

Figure 4: A rendering of the custom microscope stage used for experiments. The stage (a) and the piece used to hold the wires and reference electrode in position (b) were designed in OnShape and 3D printed using polylactic acid. Plastic screws threaded with wire were positioned using the holder (c). The reference electrode was positioned using a different part of the holder (d).

Before each experiment, electrical contact between the wire leads and ITO surface was verified using a multimeter. Also, resistance was measured between the two ITO electrodes before beginning an experiment to ensure that the 200 µm gap contained no electrical bridging. If resistance measured greater than 0 Ω across the gap, the slide was washed as described previously and measured again. If resistance greater than 0 Ω was measured after washing steps were completed, the slide was discarded. A silver/silver chloride (Ag/AgCl) reference electrode was suspended in a 100 mM Na_2SO_4 agarose salt bridge to establish connection with the media.

Cyclic Voltammetry Protocol for FMN

Cyclic voltammetry (CV) was used to establish a manipulable flavin gradient on the custom microscope slide. In brief, a potentiostat cycled between potential that would oxidize the working and counter electrodes consecutively in a three-electrode system. The machine was operated with AfterMath Data Organization Software, version 1.2.4361 (Pine Instrument

Company; Grove City, PA, USA), and the protocol contained four segments sweeping from −0.56 V vs. SHE to +0.56 V vs. SHE at 10 mV/s. The cyclic voltammetry protocol was used on 6 µL of 10 mM FMN, prepared as previously described, pipetted onto the ITO-patterned slide in the anaerobic chamber. The FMN solution on the slide was monitored for color changes to determine if it was being reduced or oxidized, as reduced flavins appear colorless, and oxidized flavins appear yellow (R. Li *et al.*, 2012).

Chronoamperometry Protocol for Cells

When cells were present in the electrochemical system, potential was applied consistently to oxidize flavins and establish a flavin redox gradient. To set a consistent potential over time, chronoamperometry was used. The protocol comprised 3 seconds initiation time, 15 minutes of applied voltage to the working electrode at 0 V vs. Ag/AgCl (+ 0.24 V vs. SHE), and then 5 seconds relaxation time.

Data Acquisition and Analysis

Video Data

Videos recorded 30-120 seconds of video prior to voltage being applied to the system, 15 minutes of applied voltage, and then 10-20 minutes without voltage to observe changes in the system equilibrium. The frame rate was 30 frames per second (fps). The frame width was 1920, and the frame height was 1080. The iPad camera setting was 4K HD.

Analysis Software

A custom Python pipeline was developed with the assistance of University of Minnesota collaborator Julian Schwanbekck and ChatGPT, model 4o (OpenAI, 2024) to render the video data in graphical form (full code provided in Appendix A2). Each video was transformed into grayscale and a region of interest (ROI) approximately 500 µm in length and 200 µm in width was selected. The ROI was positioned so that the gap between the two electrodes was centered, and ~150 µm of each electrode was visible. To remove debris and aberrations in the video, a background subtraction step was performed and was followed by a thresholding step to reduce image noise. The resulting “adjusted ROI” was divided into equal columns along the x-axis, and the pixel intensities in each column were summed. To facilitate comparison between frames, each column-sum was normalized to the maximum column-sum calculated. As thresholding accounted for the abnormally bright edges of the ITO electrodes, a value of 0 corresponded to both the

electrode edges and empty space, and a value of 100 corresponded the highest pixel-sum intensity in the dataset. Because bacteria appeared as bright spots against a dark background on the videos, pixel intensity served as a proxy for bacterial presence, where a higher sum of pixel intensity indicated higher bacterial density. Normalized pixel intensities were measured for selected frames, and histograms were plotted to visualize spatial and temporal changes in bacterial distribution across a frame.

CHAPTER 3:
RESULTS

Experimental Verification

Generating a Flavin Redox Gradient

A controllable flavin gradient was generated using CV parameters and 10 mM FMN in SBM salts and 100 mM HEPES (Figure 5). Applying an oxidation potential (+0.24 V vs SHE) to the working electrode produced a color change, where the solution near the oxidizing electrode had a bright yellow hue (evidence of oxidized flavins) and the solution near the reducing electrode became colorless (evidence of reduced flavins) (R. Li *et al.*, 2012). A visible gradient of color (colorless to bright yellow) was present between the two electrodes.

During the CV, the applied potential alternated between cathodic and anodic phases, which consequently altered which electrode was oxidizing and which electrode was reducing. Each reversal switched the location of the yellow and colorless zones, thereby inverting the direction of the flavin gradient. The switching of the color zones occurred consistently with each cycle of the CV (Supplementary Movie 1).

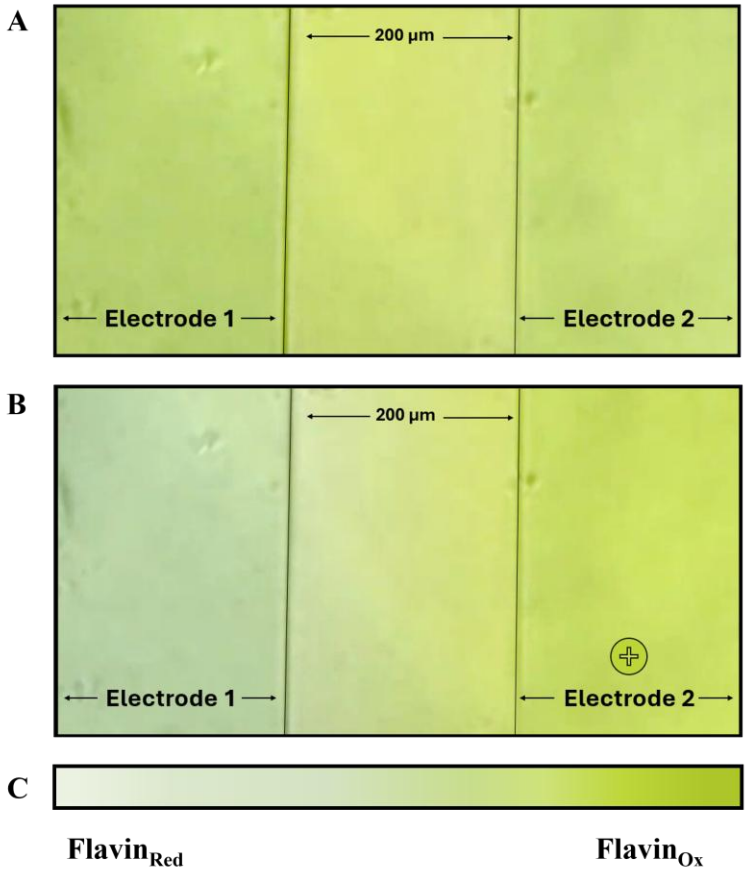

Figure 5: Flavin mononucleotide (FMN) changes color when appropriate potential is applied. 6 µL of 10 mM FMN in SBM salts and HEPES buffer was applied to a specialized glass slide with ITO electrodes (Electrode 1 and Electrode 2, respectively) on its surface. A 200-µm gap separated the ITO electrodes. **(A)** FMN appears uniformly yellow when no potential is applied. **(B)** Oxidizing potential is applied to the working electrode (Electrode 2) at + 0.24 V vs. SHE (indicated by plus symbol on Electrode 2). At + 0.24 V vs. SHE, Electrode 1 becomes reducing, and Electrode 2 becomes oxidizing. The FMN solution becomes colorless at Electrode 1 and remains vibrantly yellow at Electrode 2. **(C)** A legend correlating the gradient color to redox state indicates that a colorless solution signifies that FMN is reduced, and a vibrant yellow solution signifies that FMN is oxidized.

For all experiments with cells, the media appeared homogenously yellow throughout the imaging field in the absence of applied potential. When potential was applied to the experimental system, a color change was observed at the working electrode for WT and Δ*cheA-3* mutants. No significant color change was observed with the ΔEET strain.

S. oneidensis MR-1

The Response of *S. oneidensis* MR-1 to a Poised Electrode

To assess the response of *S. oneidensis* to a poised electrode, a culture of wild-type (WT) *S. oneidensis* MR-1 was grown and prepared for experimentation as described in the methods. After dilution steps, the concentrations in the anaerobic microscopy sample were estimated to be 1.3 mM fumarate, 0.6 mM lactate, and 9.0 mM FMN, with an estimated cell density of 0.03. The sample was pipetted onto the prepared ITO-patterned slide and visualized with and without +0.24 V vs SHE applied to the system using chronoamperometry (Supplementary Movie 2).

When no potential was applied, the media appeared homogenously yellow, and cells displayed their biased, random walk throughout the image area. As the working electrode was poised to +0.24 V vs. SHE, the liquid around the counter electrode became colorless. In contrast, the liquid around the working electrode remained a vibrant yellow, with the color persisting for all 15 minutes that the potential was applied.

In addition to the observable color change between the two electrodes, motility also differed between the counter and working electrodes (Figure 6). Once potential was applied, cells congregated at the working electrode and rarely swam back across the halfway point separating the counter and working electrodes. They instead remained above the working electrode or within ~ 100 μm of its edge. When shifts in the liquid occurred, the phenotype of congregation at the working electrode persisted (Figure 6A). Also, the cells at the counter electrode began to swim more slowly, and the dominant phenotype at the counter electrode became non-motile over the 15 minutes of applied potential. In contrast, cells near the working electrode qualitatively increased their observable swim speeds and reversed their swim direction more frequently (Supplementary Movie 2). Cell density continued to increase at the working electrode over the course of the applied voltage (Figure 7).

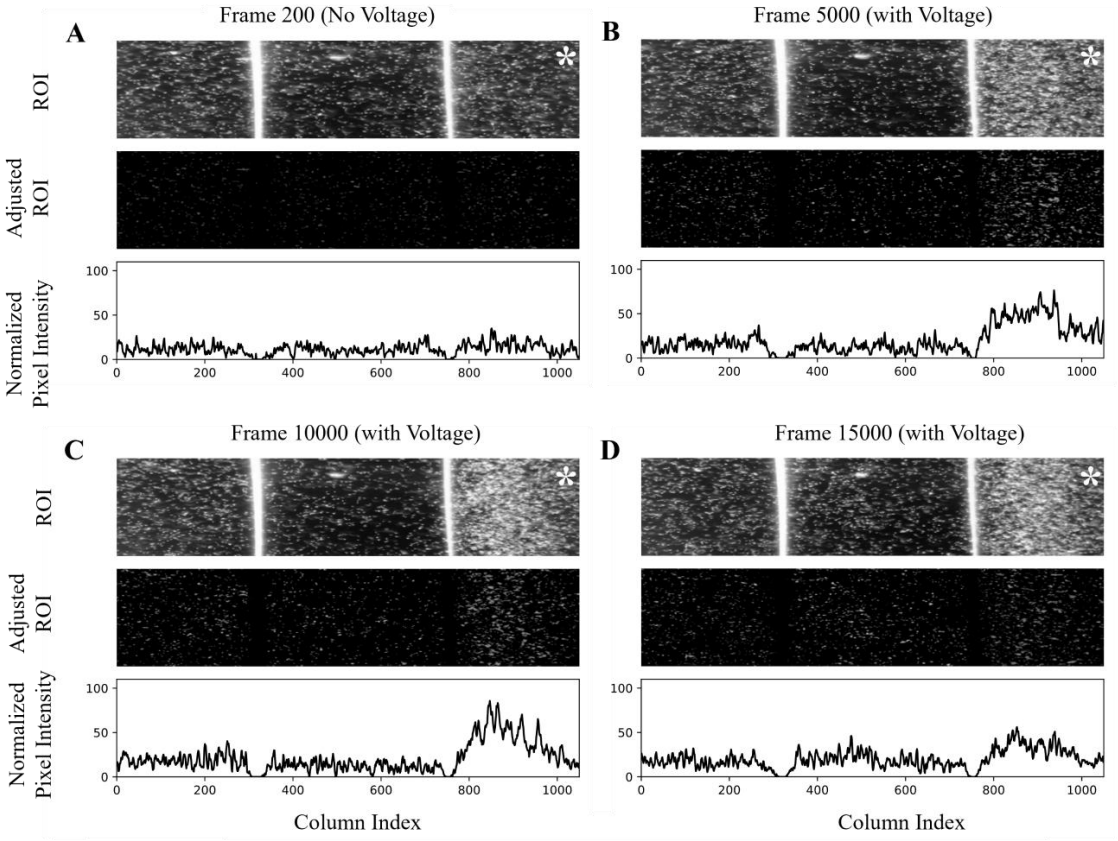

Figure 6: Wild-type *S. oneidensis* cells increase in density at the poised working electrode. Videos of *S. oneidensis* motility in response to a poised electrode were taken over the course of fifteen minutes. The image was distilled into a series of frames using a custom Python pipeline, and a region of interest (ROI) was isolated from selected frames, with the working electrode denoted by a white asterisk (*) (A-D, **top panel**). The ROI was then adjusted to remove noise and standardize the image (Adjusted ROI, A-D, **middle panel**). Finally, a histogram of pixel brightness was calculated across column indices of the frame and normalized to the maximum pixel brightness across the frames (A-D, **bottom panel**). The x-axis above each panel includes the counter electrode (column index 0-325), inter-electrode gap (325-740), and working electrode (740-1020). **(A)** Frame 200: no voltage is applied to the electrode, and cell density is relatively uniform throughout the ROI. **(B)** Frame 5,000: the working electrode is poised to +0.24 V vs. SHE. **(C)** Frame 10,000: working electrode remains poised to +0.24 V vs. SHE. **(D)** Frame 15,000: a shift in the liquid is observed. The working electrode remains poised to +0.24 V vs. SHE.

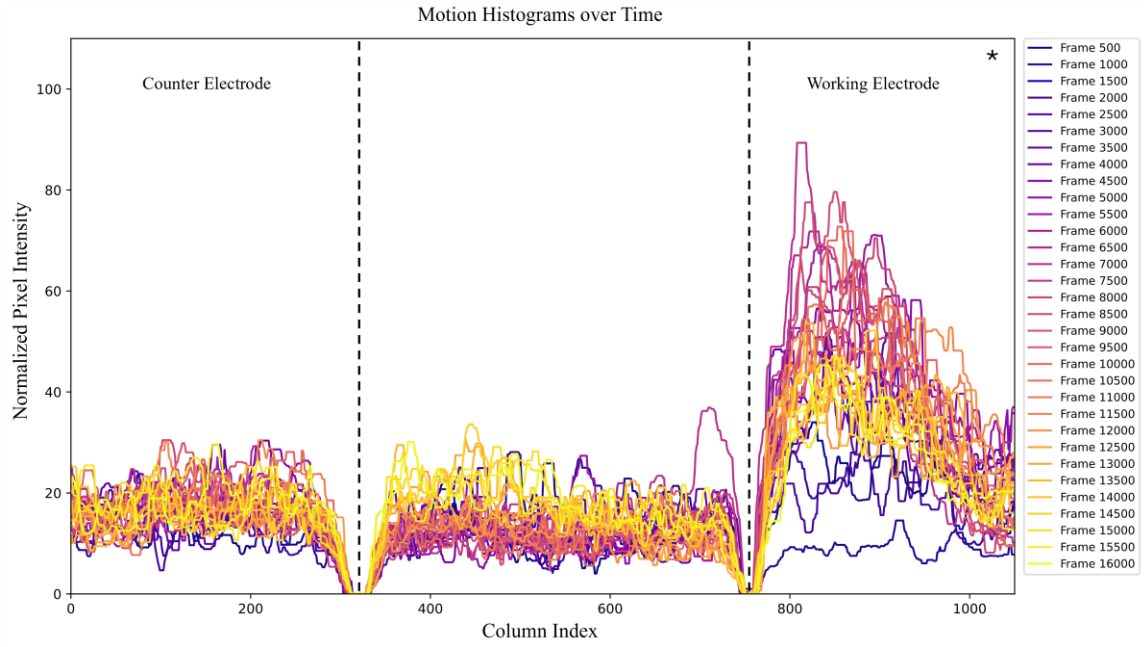

Figure 7: Wild-type *S. oneidensis* cells maintain increased density at the poised working electrode over time. Histograms of WT *S. oneidensis* cell densities across a region of interest were computed. Line colors represent timepoints beginning from earlier timepoints (frame 500, dark purple) to later timepoints (frame 16000, yellow). The x-axis includes the counter electrode (column index 0-325), inter-electrode gap (325-740), and working electrode denoted by an asterisk (740-1020). Cells maintain a higher density at the working electrode than the counter electrode over the course of the applied voltage.

After the applied current ceased, the phenotype of congregation near the working electrode changed (Supplementary Movie 2). Cells slowly dispersed from the working electrode. They made longer runs and more frequently crossed the halfway point between the working and counter electrodes. Furthermore, the color difference between the electrodes also diminished once the current ceased. The solution became yellow throughout the field of vision after 15-20 minutes without any voltage applied to the system.

Changing the Direction of Electron Flow for *S. oneidensis* MR-1

To assess the effect of liquid drift on the cells' congregation, the counter and working electrodes were switched on the potentiostat (Supplementary Movie 3). The phenotype of increased swim speeds and reversal frequencies now occurred around the newly poised working electrode. The cells again congregated near the new working electrode, and the color of the

solution at the working electrode remained a bright yellow in contrast to the counter electrode's colorless hue (Figures 8 and 9).

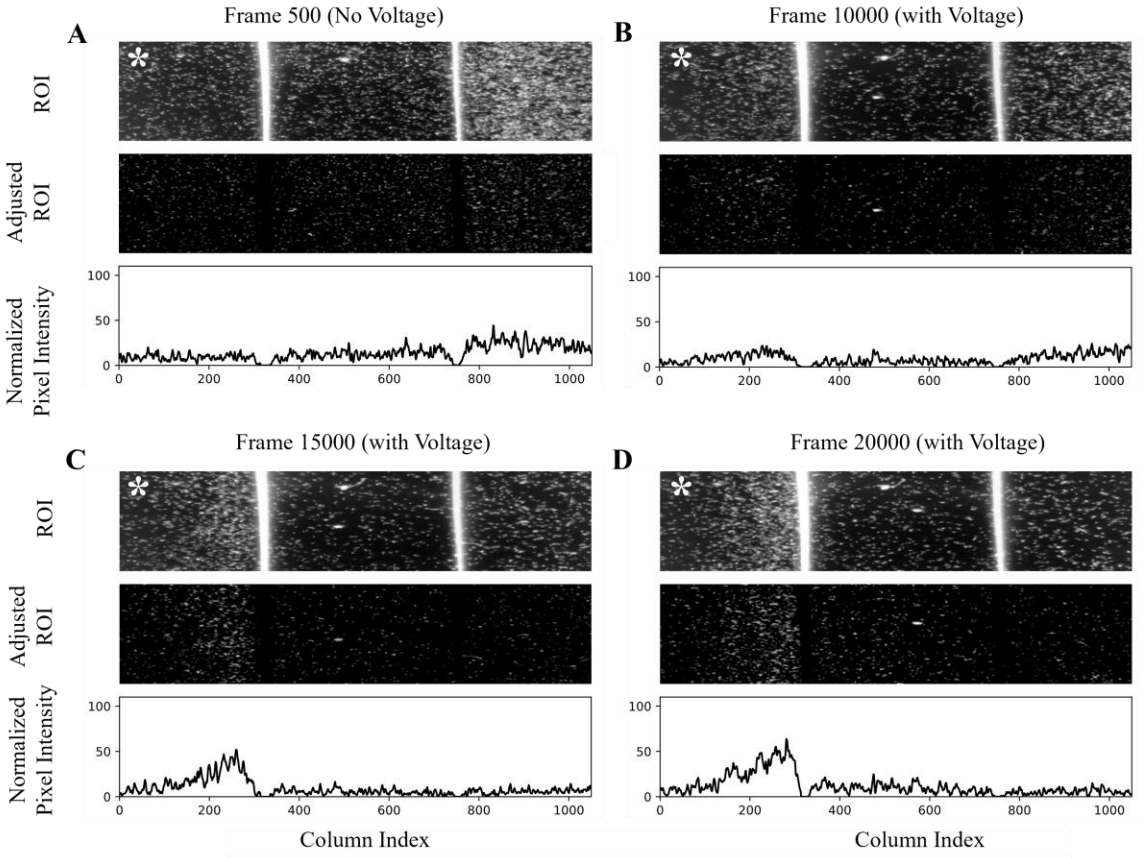

Figure 8: Wild-type *S. oneidensis* cells respond to change in direction of electron flow. Videos of *S. oneidensis* motility in response to a poised electrode were taken over the course of fifteen minutes. The image was distilled into a series of frames using a custom Python pipeline, and a region of interest (ROI) was isolated from selected frames, with the working electrode indicated by a white asterisk (*) (A-D **top panel**). The ROI was then adjusted to remove noise and standardize the image (Adjusted ROI, A-D **middle panel**). Finally, a histogram of pixel brightness was calculated across column indices of the frame and normalized to the maximum pixel brightness across the frames (A-D **bottom panel**). The x-axis above each panel includes the newly poised working electrode (column index 0-325), inter-electrode gap (325-740), and counter electrode (740-1020). **(A)** Frame 500: no voltage is applied to the electrode, and cell density remains slightly elevated between electrodes after the previous run of the experiment. **(B)** Frame 10,000: the left electrode is poised to +0.24 V vs. SHE. Cell density is relatively uniform throughout the ROI. **(C)** Frame 15,000: the left working electrode remains poised to +0.24 V vs.

SHE. Cells begin to increase in density at the poised electrode. **(D)** Frame 20,000: working electrode remains poised to +0.24 V vs. SHE. Cells continue to increase in density.

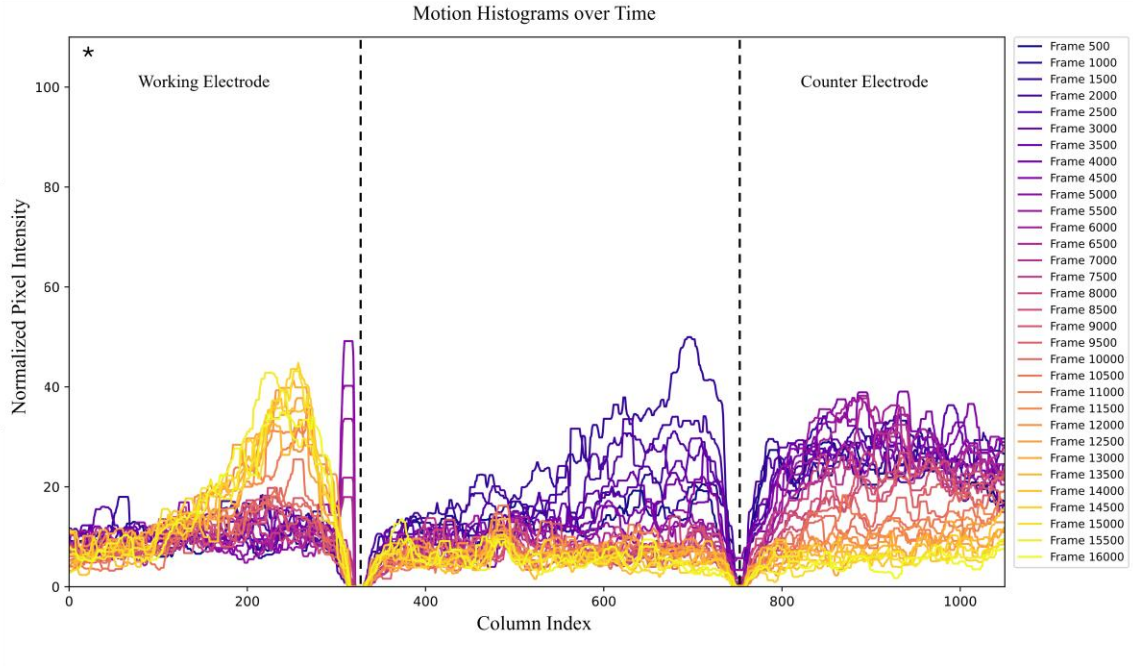

Figure 9: Wild-type *S. oneidensis* cells respond to change in electron flow over time. Histograms of WT *S. oneidensis* cell densities across the region of interest were computed. The edge of the working electrode extends from column index 0 to 325 and is indicated by an asterisk (*). Line colors represent timepoints beginning from earlier in the video (frame 500, dark purple) to later in the video (frame 16000, yellow). Around frame 500 cells are at a higher density between indices 740 and 1020. As the video progresses, cell density becomes higher between indices 0 and 325 at the newly poised working electrode.

S. oneidensis Mutant Deficient in Chemotaxis

The Response of *S. oneidensis* Δ*cheA-3* to the Poised Electrode

To evaluate the effect of the shewanellae chemotaxis pathway on the phenotype of electrokinesis, a mutant deficient in chemotaxis was used: *S. oneidensis* Δ*cheA-3*. After dilutions, the microscopy sample had estimated concentrations of 5 mM fumarate, 2.5 mM lactate, 7.5 mM FMN, and an estimated cell density of 0.09. Though the concentrations of fumarate, lactate, and FMN differed from the experiment performed with wild-type *S. oneidensis*, motility for the *cheA-3* mutant was confirmed with 5 mM fumarate and 2.5 mM lactate. Also, the concentration of 7.5 mM FMN still allowed sufficient visualization of the FMN color changes.

When no voltage was applied, the media appeared homogenously yellow (Supplementary Movie 4). The Δ*cheA-3* cells displayed a smooth-swimming phenotype of motility, *i.e.* there was a complete lack of flagellar reversals. As potential was applied to the system, the solution around the counter electrode became colorless and the solution around the working electrode remained a vibrant yellow, which persisted for all 15 minutes that the current was applied.

There was also a change in swim speeds observed for the Δ*cheA-3* mutant. The cells at the counter electrode began to swim more slowly, and cells near the working electrode increased their visible swim speeds. Observationally, it appeared that the increase in swim speeds was not as large or as widespread as it was for WT cells, however, more analytics are needed to statistically validate this observation.

Although swim speeds increased at the working electrode, there was no congregation around or near it (Figures 10 and 11). Cells indiscriminately crossed the 200 μm gap between the working and counter electrodes, showing no radius-dependent phenotype of congregation that was observed with WT cells. Also, a small subset of Δ*cheA-3* cells at the counter electrode remained motile, which was not observed with WT cells.

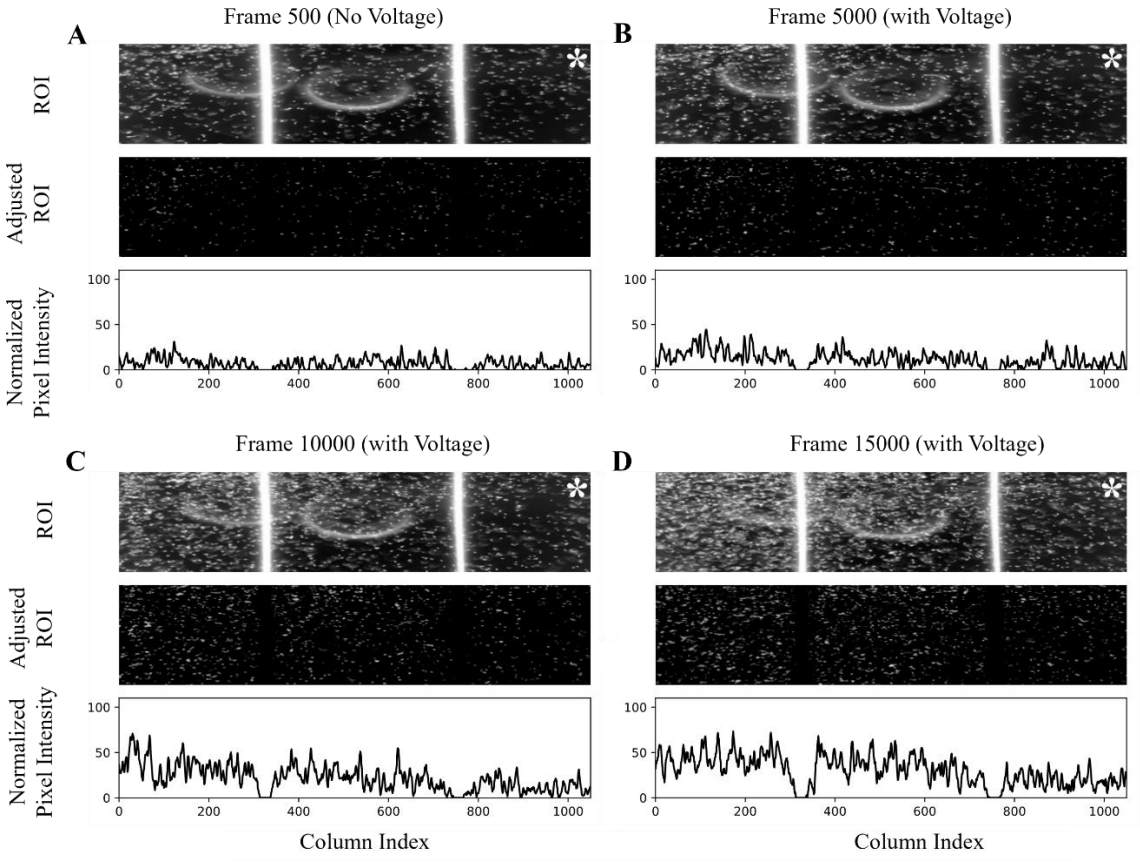

Figure 10: *S. oneidensis* Δ*cheA-3* does not congregate at the working electrode. Videos of *S. oneidensis* Δ*cheA-3* motility in response to a poised electrode were taken over the course of 15 minutes. The image was distilled into a series of frames using a custom Python pipeline, and a region of interest (ROI) was isolated from selected frames (A-D **top panel**). The ROI was then adjusted to remove noise and standardize the image, and the working electrode was denoted with a white asterisk (*) (Adjusted ROI, A-D **middle panel**). Finally, a histogram of pixel brightness was calculated across column indices of the frame and normalized to the maximum pixel brightness across the frames (A-D **bottom panel**). The x-axis above each panel includes the counter electrode (column index 0-325), inter-electrode gap (325-740), and working electrode (740-1020). **(A)** Frame 500: no voltage is applied to the electrode, and cell density is relatively uniform throughout the ROI. **(B)** Frame 5,000: the working electrode is poised to +0.24 V vs. SHE and remains as such for C-D. **(C)** Frame 10,000 is selected for observation. A drift of the liquid results in increased cell density between indices 0 and 500. **(D)** Frame 15,000 is selected for observation.

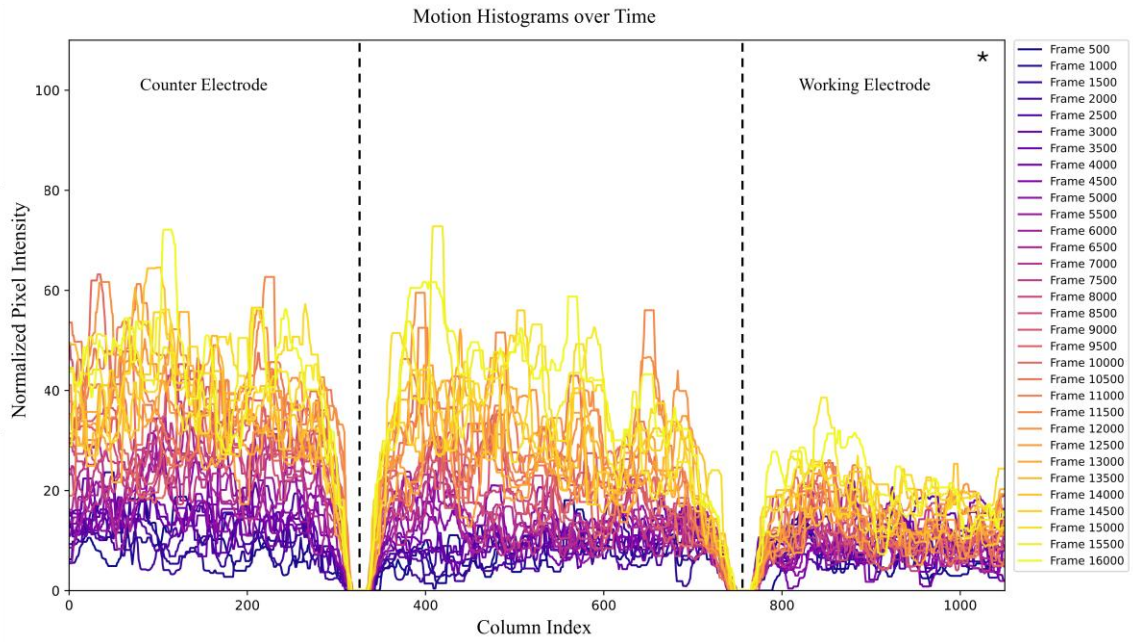

Figure 11: *S. oneidensis* Δ*cheA-3* does not congregate at the working electrode over time. Histograms of *S. oneidensis* Δ*cheA-3* cell densities across the region of interest were computed. The x-axis includes the counter electrode (column index 0-325), inter-electrode gap (325-740), and working electrode denoted by an asterisk (740-1020). Line colors represent timepoints beginning from earlier frames (frame 500, dark purple) to later frames (frame 16000, yellow). Cells density remains low at the working electrode. Cell density appears higher at indices 0 to 700 due to abiotic factors.

Changing the Direction of Electron Flow for *S. oneidensis* Δ*cheA-3*

To assess the effect of liquid drift on cell density, the counter and working electrodes were switched on the potentiostat (Supplementary Movie 5). Once switched, swim speeds increased at the new working electrode. However, there remained no indication of congregation at the working electrode (Figures 12 and 13)

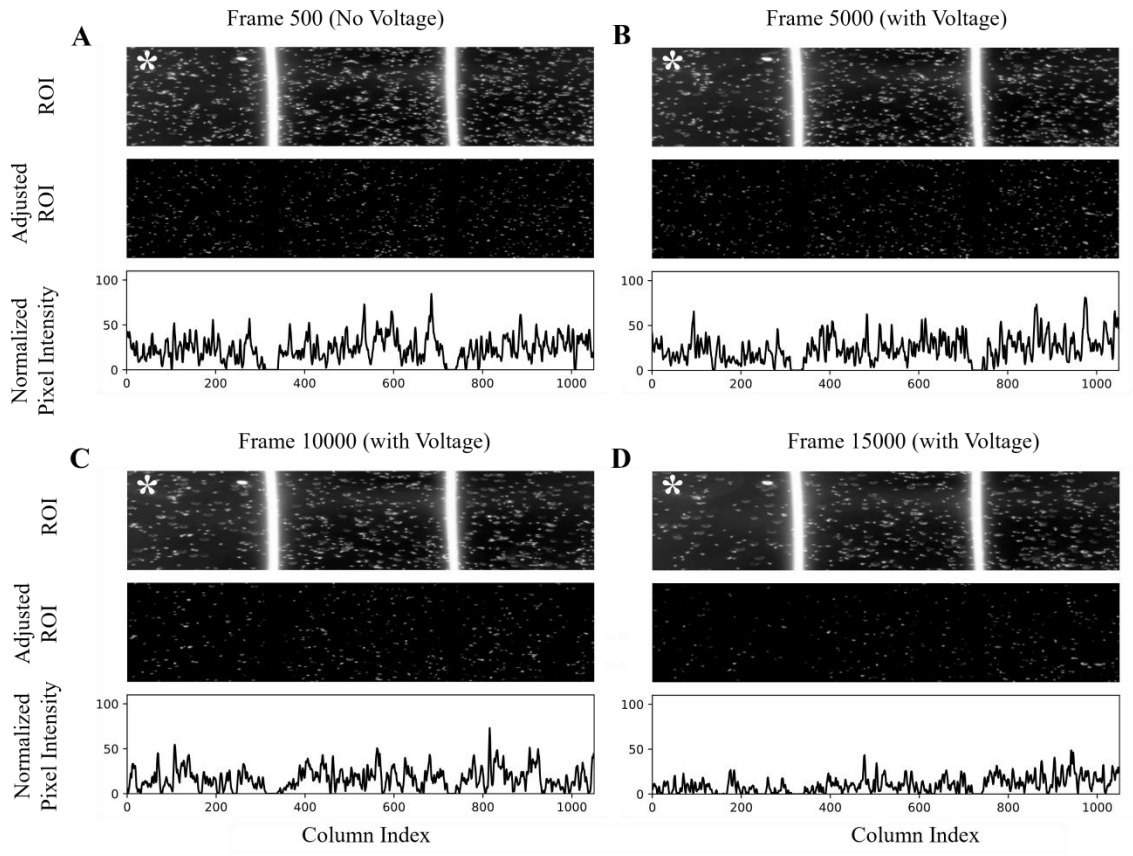

Figure 12: *S. oneidensis* Δ*cheA-3* cell density remains relatively uniform regardless of the working electrode. Videos of *S. oneidensis* Δ*cheA-3* motility in response to a poised electrode were taken over the course of fifteen minutes. The image was distilled into a series of frames using a custom Python pipeline, and a region of interest (ROI) was isolated from selected frames, with the working electrode denoted using a white asterisk (*) (A-D **top panel**). The ROI was then adjusted to remove noise and standardize the image (Adjusted ROI, A-D **middle panel**). Finally, a histogram of pixel brightness was calculated across column indices of the frame and normalized to the maximum pixel brightness across the frames (A-D **bottom panel**). The x-axis of each panel includes the working electrode (column index 0 to 325), inter-electrode space (325 to 740), and counter electrode (740 to 1020). **(A)** Frame 500: no voltage is applied to the electrode, and cell density is relatively uniform throughout the ROI. **(B-D)** Frames 5,000, 10,000 and 15,000 are selected for observation: the working electrode is poised to +0.24 V vs. SHE and cell density remains relatively uniform.

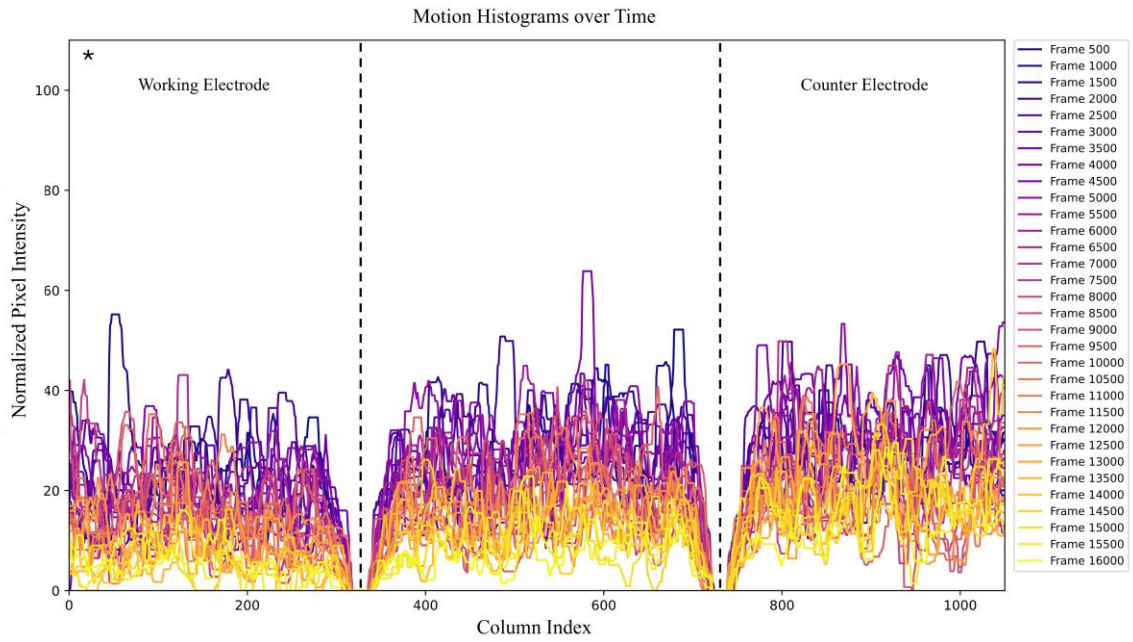

Figure 13: *S. oneidensis* Δ*cheA-3* cell density remains relatively uniform over time, regardless of the working electrode. Histograms of *S. oneidensis* Δ*cheA-3* cell densities were computed across the region of interest. The x-axis includes the working electrode (column index 0 to 325), indicated by an asterisk (*), the inter-electrode space (325 to 740), and the counter electrode (740 to 1020). Line colors represent timepoints beginning from earlier frames (frame 500, dark purple) to later frames (frame 16000, yellow). Cells density remains relatively homogenous across the distribution of the frame, regardless of which electrode is the working electrode.

Experimental Aberrations

Additional experiments were conducted to decrease the cell density of the Δ*cheA-3* microscopy sample and standardize the concentrations of media components across treatments. However, the recordings were interrupted with gas production at the counter electrode, strong electrical fields that artificially altered the bacteria's path of motion, and discoloration of both electrodes' physical surfaces. Upon investigating the source of the error, there appeared little contact between the agarose salt bridge and the liquid under the coverslip. The microscope slide was discarded due to physical aberrations, and the video data was not analyzed. Future experiments will be performed to directly compare the *cheA-3* mutant with WT *S. oneidensis* at the same concentration of cells in addition to the same concentrations of electron donor, electron acceptor, and FMN.

S. oneidensis Mutant Deficient in EET

To evaluate the effect of EET on electrolocation, a mutant of *S. oneidensis* lacking EET capability was tested: *S. oneidensis* ΔEET. The microscopy sample contained calculated concentrations of 2.0 mM fumarate, 1.0 mM lactate, and 9.9 mM FMN, and had an estimated cell density of 0.03. Though the working concentrations of fumarate and lactate differed from the experiment performed with *S. oneidensis* and *S. oneidensis* Δ*cheA-3*, motility for the ΔEET strain was confirmed with 2.0 mM fumarate and 1.0 mM lactate.

When no voltage was applied, the media appeared homogenously yellow (Supplementary Movie 6). As potential was applied to the system, the solution around the counter electrode became colorless, and the solution around the working electrode remained a vibrant yellow. The color change persisted for all 15 minutes that the current was applied, however it was not as intense of a color change as observed in previous experiments with other strains.

Motility for the ΔEET strain was lower than both the WT and Δ*cheA-3* cells. Though the sample was tested for sufficient motility before the experiment began, it was also tested after experiments were completed. After four hours in the anaerobic chamber, the dominant phenotype of the cells was non-motile (data not shown), and there were fewer cells in the field of view than expected from the dilution calculations. Also, the field of vision was more gold in color than blue, which may imply that the microscope settings were different than in previous experiments.

As potential was applied to the system, there was a slight difference in media coloration between the counter and working electrodes as observed with the human eye, but it was not pronounced. With visual observation of cell motility, the applied potential had little to no effect on cell swim speeds or run lengths (Figures 14 and 15). More experiments in combination with statistical analyses are needed to determine if the EET mutant displays phenotypic differences at the working electrode.

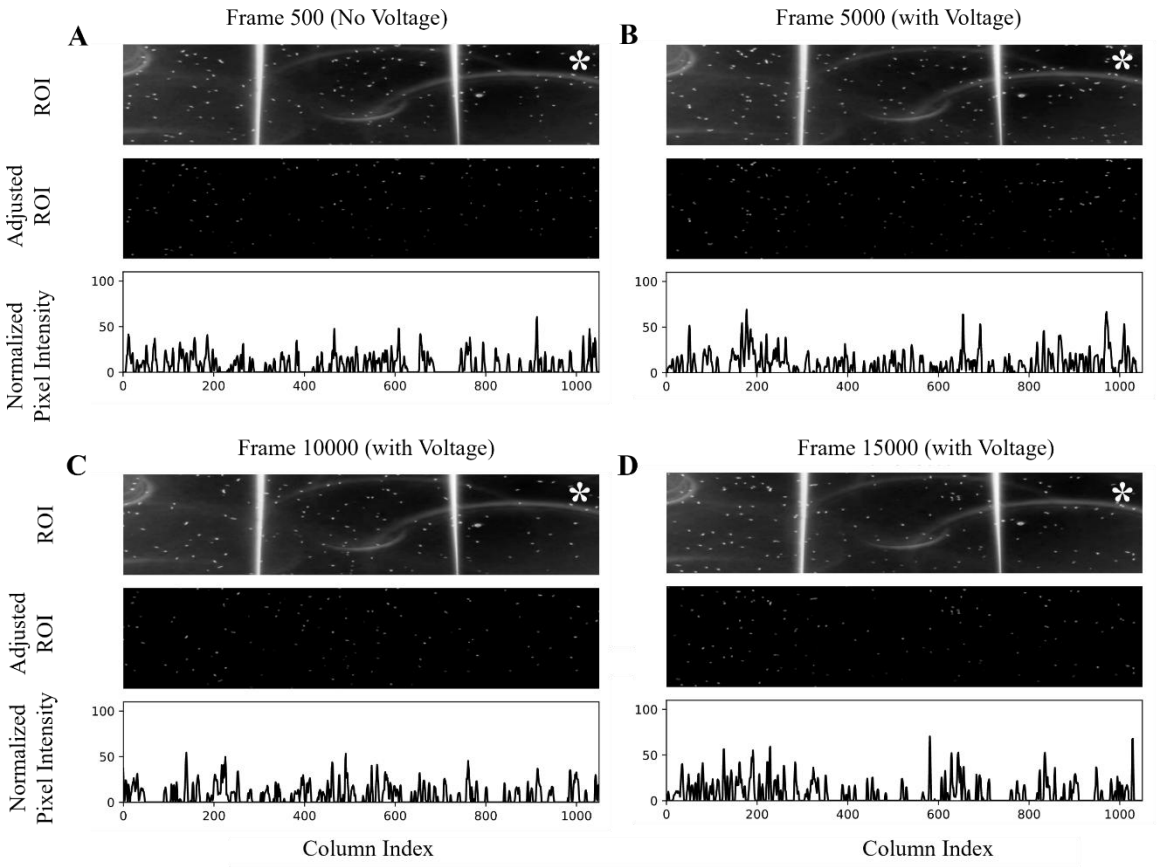

Figure 14: The *S. oneidensis* ΔEET strain does not appear to congregate near the working electrode. Videos of *S. oneidensis* ΔEET motility in response to a poised electrode were taken over the course of fifteen minutes. The image was distilled into a series of frames using a custom Python pipeline, and a region of interest (ROI) was isolated from selected frames (A-D **top panel**). The ROI was then adjusted to remove noise and standardize the image, and the working electrode was denoted with a white asterisk (*) (Adjusted ROI, A-D **middle panel**). Finally, a histogram of pixel brightness was calculated across column indices of the frame and normalized to the maximum pixel brightness across the frames (A-D **bottom panel**). The x-axis above each panel includes the counter electrode (column index 0-325), inter-electrode gap (325-740), and working electrode (740-1020). **(A)** Frame 500: no voltage is applied to the electrode. **(B-D)** Frames 5,000, 10,000, and 15,000 are selected for observation, respectively. The working electrode is poised to +0.24 V vs. SHE, and cell density remains relatively uniform throughout the ROI.

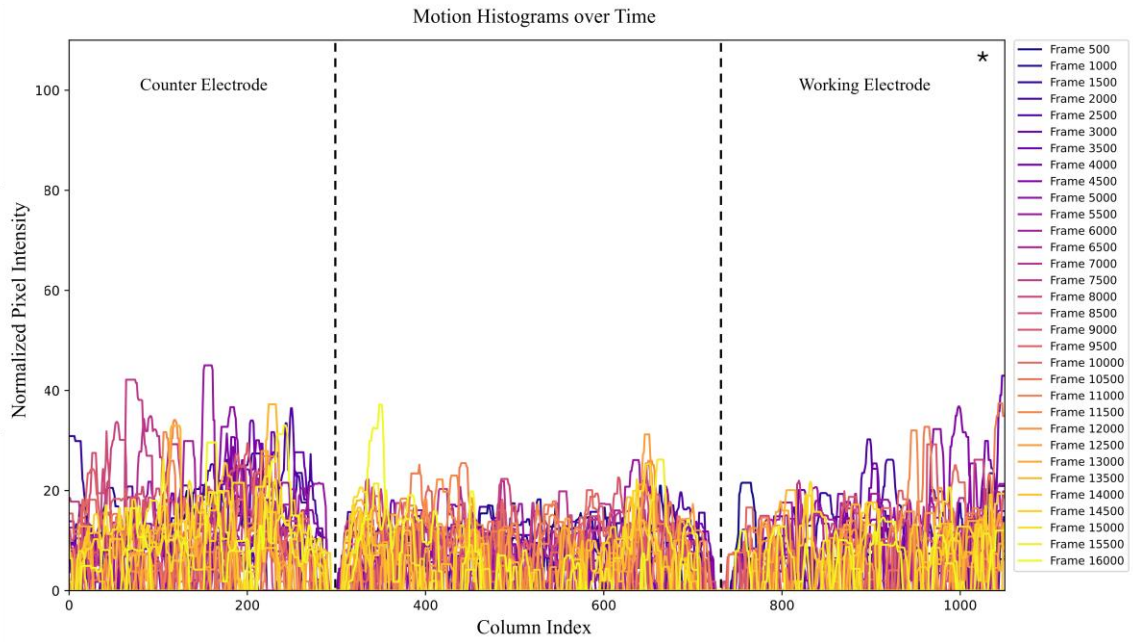

Figure 15: The *S. oneidensis* ΔEET strain does not congregate near the poised working electrode over time. Histograms of *S. oneidensis* ΔEET cell densities were computed for the region of interest. The x-axis includes the counter electrode (column index 0-325), inter-electrode space (325-740), and working electrode denoted by an asterisk (740-1020). Line colors represent timepoints beginning from earlier frames (frame 500, dark purple) to later frames (frame 16000, yellow). Cells density does not shift toward the working electrode significantly over the course of the applied voltage.

Changing the Direction of Electron Flow for the *S. oneidensis* ΔEET Strain

To assess the effect of liquid drift on cell density, the counter and working electrodes were switched on the potentiostat (Supplementary Movie 7). Upon changing which electrode was reducing and which electrode was oxidizing, no change in swim speed or reversals were observed, and no indication of congregation at the working electrode was observed (Figures 16 and 17). Again, only a slight color change was observed at the working electrode.

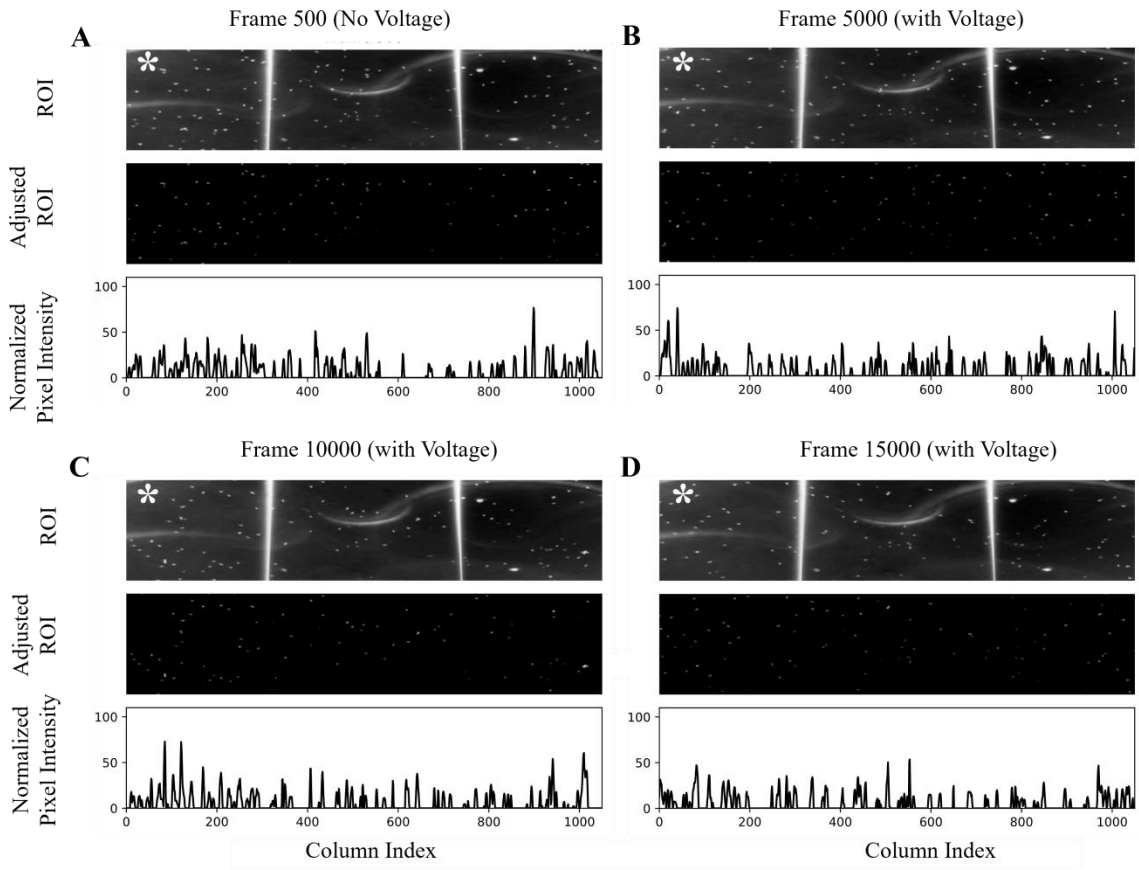

Figure 16: *S. oneidensis* ΔEET cells do not respond to change in direction of electron flow. Videos of *S. oneidensis* ΔEET motility in response to a poised electrode were taken over the course of fifteen minutes. The image was distilled into a series of frames using a custom Python pipeline, and a region of interest (ROI) was isolated from selected frames, with the working electrode denoted using a white asterisk (*) (A-D **top panel**). The ROI was then adjusted to remove noise and standardize the image (Adjusted ROI, A-D **middle panel**). Finally, a histogram of pixel brightness was calculated across column indices of the frame and normalized to the maximum pixel brightness across the frames (A-D **bottom panel**). The x-axis of each panel includes the working electrode (column index 0 to 325), inter-electrode space (325 to 740), and counter electrode (740 to 1020). **(A)** Frame 500: no voltage is applied to the electrode, and cell density is relatively uniform throughout the ROI. **(B-D)** Frames 5,000, 10,000 and 15,000 are selected for observation: the working electrode is poised to +0.24 V vs. SHE and cell density remains relatively uniform.

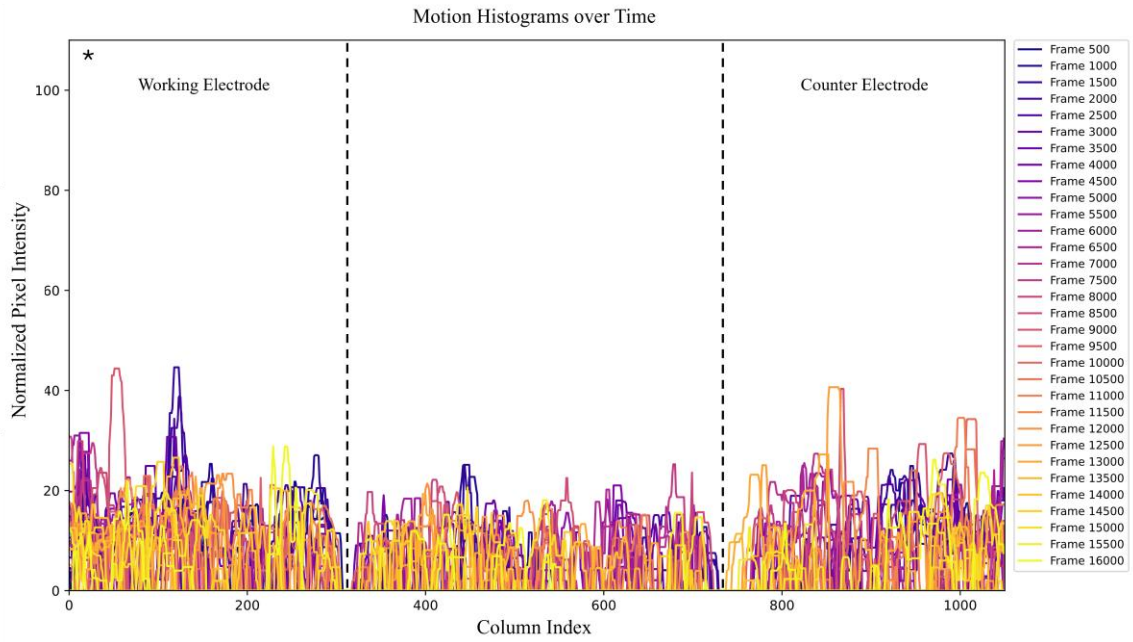

Figure 17: *S. oneidensis* ΔEET cells maintain relatively consistent cell density over time, regardless of which electrode is poised. Histograms of *S. oneidensis* cell densities were computed. The x-axis includes the working electrode (column index 0 to 325) as indicated by an asterisk (*), the inter-electrode space (325 to 740), and the counter electrode (740 to 1020). Darker lines (purple, frame 500) indicate an earlier timepoint in the video recording. Lighter lines (yellow, frame 16000) indicate a later timepoint in the video recording. As the video progresses, there appears to be no dominant change in cell densities near the working electrode.

CHAPTER 4:
DISCUSSION

Through a combination of microscopy, electrochemistry, and analytical software, this study investigated the hypothesis that oxidized flavins serve as a chemotactic signal for *S. oneidensis* navigation toward insoluble electron acceptors. By providing proof of concept experimental design, initial tests with mutants deficient in chemotaxis and EET functionality, and establishing a pipeline for future analyses, this study set the stage for deeper mechanistic studies on shewanellae redox sensing.

Flavin Redox Gradient

First, a controllable gradient of reduced to oxidized flavins was established. Since reduced flavins appear colorless and oxidized flavins appear yellow, visualizing a distinct color change upon applying potential indicated the redox state of the flavins (R. Li *et al.*, 2012). A flavin concentration in the millimolar range was chosen for the experiments to increase the ease of visibility. As expected, when the working electrode was poised to an oxidizing potential in the experimental system, the flavin solution became colorless at the counter electrode and yellow at the working electrode, signs of reduced and oxidized FMN, respectively (Figure 5). A gradient of reduced to oxidized FMN was also visualized, as the color gradient extended from the counter to the working electrode transitioning from colorless to yellow as it neared the working electrode. The direction of the gradient was controlled by manipulating the direction of electron flow and changing which electrode was reducing and which electrode was oxidizing. All experiments for *S. oneidensis* MR-1 and *S. oneidensis* Δ*cheA-3* had clear zones of oxidation at the working electrode as indicated by the yellow color change. However, the experiments performed with *S. oneidensis* ΔEET did not have as distinct of a color change, which may indicate a faulty electrochemical connection and thus a lack of the flavin gradient forming.

Analysis of Motility Responses

S. oneidensis MR-1 Congregated at the Poised Electrode

Testing the motility behavior of *S. oneidensis* MR-1 in the electrochemical system revealed that the WT strain responds to the presence of an electrode poised at + 0.24 V vs SHE by increasing swim speed and congregating at the poised electrode surface. This behavior aligns with the electrokinetic phenotype described by Harris *et al.* (2010). Flavin oxidation was visually

apparent at the working electrode, as indicated by the development of a bright yellow color near its surface.

Quantitative image analysis showed that cell density at the working electrode increased within ~5000 frames (~2.78 min after video start, ~2.62 min after potential was applied; Figure 6). Elevated cell density persisted over time (Figure 7), suggesting a sustained motility response. The highest peaks in pixel intensity were observed around frame 5000, just prior to a rapid shift in the medium due to evaporation. After this point, frames represent a population of cells that are more dispersed from the electrode surface and are navigating back toward the edge of the electrode, where they congregate at the highest density. Despite the disturbance to the media, the phenotype persisted, with cell density remaining higher at the working electrode compared to the counter electrode.

As cell density increased at the working electrode, it was observed that WT *S. oneidensis* cells crossed the 200 μm gap separating the counter electrode and the working electrode to move toward the working electrode. Once they reached it, however, they remained either on top of its surface or within ~100 μm of its edge. If cells swam away from the working electrode toward the counter electrode, they only swam ~100 μm into the gap before reversing their direction multiple times to again near the working electrode. This observation is consistent with the inflection point of the flavin redox gradient that is visualized in Figure 5, where the dominant redox state of flavins changes from reduced to oxidized between the two electrodes around the 100 μm mark. The fact that WT *S. oneidensis* cells reached this threshold and reversed direction to return toward the working electrode suggests that oxidized flavins may be the critical component in the congregation behavior observed near the working electrode.

When the direction of electron flow was reversed and the working electrode was switched to be on the opposite side of the slide, WT *S. oneidensis* reoriented its motility pattern accordingly. Initially, cell density remained higher near the original working electrode (Figure 8A), reflecting the previously oxidizing conditions. As the newly positioned working electrode became poised at +0.24 V vs SHE, cells navigated toward the new location, increasing density on the left side of the frame (Figures 8B–D). Later frames were selected for analysis in Figure 8 (Frames 10,000, 15,000 and 20,000 of 8B-D, respectively), because more time was needed to illustrate the restoration of congregation after switching which electrode was the working electrode. The shift in distribution was also captured in the temporal trends shown in Figure 9.

An unexpected peak in pixel intensity near column index 320 of figure 9 (Frame ~5,000) was traced to an artifact in the image thresholding function, where the edge of the electrode was

incorrectly included in pixel counts and histogram calculations (Figure AI). This feature was not caused by cell behavior and does not affect the interpretation of motility trends.

S. oneidensis Δ*cheA-3* Does Not Congregate at the Poised Electrode

In contrast to the WT cells, *S. oneidensis* Δ*cheA-3* cells did not congregate at the working electrode. Consistent with prior observations of Δ*cheA-3* mutants (Harris *et al.*, 2012; J. Li *et al.*, 2007), the cells exhibited a smooth-swimming phenotype, with straight runs and no flagellar reversals throughout the duration of observation. Though there were no flagellar reversals, the Δ*cheA-3* strain did show a localized increase in swim speed at the working electrode upon application of +0.24 V vs SHE. However, the change in swim speed appeared less pronounced and less widespread than in the WT cell population, though additional quantitative analyses are needed to confirm this observation. Flavin oxidation at the working electrode was evident by the characteristic bright yellow coloration, and a visual gradient was present. However, Δ*cheA-3* cells did not respond to the gradient through congregation and indiscriminately crossed the 200 μm gap separating the two electrodes.

The microscopy culture for the *S. oneidensis* Δ*cheA-3* strain differed in fumarate, lactate, and FMN concentrations compared to the WT treatment due to adjustments in dilution factors to optimize cell densities for imaging. However, all concentrations remained within the millimolar range and were not expected to account for the absence of congregation in the Δ*cheA-3* strain, since the Δ*cheA-3* strain was still motile in the media, and FMN oxidation was still observed via color change. Regardless, future studies will standardize the media components across replicates to ensure consistency and comparability.

Debris present in the ROI (Figure 10A-D, top panel) was successfully excluded from quantitative analysis when creating the adjusted ROI (Figure 10A-D, middle panel). A higher initial cell density on the left side of the frame (column indices 0-750) was caused by liquid drift, which deposited more cells in that region and was not attributed to cell motility (Figures 10 and 11). When the direction of electron flow was reversed so that the working electrode became the electrode on the left (column indices 0-325) (Figure 12), the microscope imaging field was also changed slightly to avoid the area of large liquid drift and artificially high cell density. Reversing the direction of electron flow did not lead to congregation at the working electrode, and Figure 13 shows a more even distribution cell density between the two electrodes, as was expected for the Δ*cheA-3* strain. When the polarity of the electrodes was changed, a localized increase in swim speed for the Δ*cheA-3* strain was again observed at the working electrode.

Though the Δ*cheA-3* mutant did not exhibit congregation at the working electrode, the deletion of *cheA-3* leads to a smooth-swimming phenotype, meaning that it is impossible for Δ*cheA-3* cells to reverse the direction of their flagellar rotation. Thus, the absence of congregation may be due to the mutant's smooth-swimming phenotype rather than a complete loss of electrolocation capability. Future studies are needed with complemented *cheA-3* strains to determine whether restoring the chemotaxis machinery also restores congregation behavior.

S. oneidensis Lacking EET Functionality

The *S. oneidensis* ΔEET strain, lacking key cytochromes required for extracellular electron transfer, did not significantly increase in cell density nor swim speed at the working electrode. However, interpretation of results using the ΔEET strain were limited due to experimental challenges. In addition to the concentrations of fumarate, lactate, and FMN being different in the ΔEET microscopy culture than in both the WT and Δ*cheA-3* cultures, the ΔEET microscopy culture also had a low cell density and few motile cells. As a result, the sample size available for analysis was low. Future experiments will be repeated with consistent culture concentrations and a higher cell density.

Another experimental challenge with the *S. oneidensis* ΔEET strain was that it lacks cytochromes necessary for EET, including the fumarate reductase FccA. Without FccA, the cells cannot metabolize the fumarate present in the media to generate proton motive force. Thus, the cells would have limited energy available for motility under the conditions tested. Future studies would benefit from shortening the incubation time in anaerobic media or using a strain that is inhibited farther up in the EET chain, such as a strain lacking *mtrABC* and *mtrDEF* gene clusters.

CHAPTER 5:
CONCLUSIONS AND FUTURE DIRECTIONS

Conclusion

Many studies have probed the remarkable respiratory versatility of *Shewanella* species. Through a system of EET proteins, the model organism *S. oneidensis* MR-1 transfers electrons through the barrier of its outer membrane to insoluble electron acceptors outside of the cell. By overcoming the barrier of the outer membrane, EET broadens the range of electron acceptors that *S. oneidensis* can use for respiration and allows the organism to survive in rapidly changing, diverse redox environments (Gralnick & Bond, 2023). However, mysteries regarding the respiratory versatility of *S. oneidensis* remain. The classical definition of how bacteria navigate towards electron acceptors in their environment originates from the process of chemotaxis: the random, biased walk a motile cell takes up or down concentrations of chemicals in its environment (Berg, 1975). For chemotaxis to work, a gradient of chemicals must be present. However, insoluble electron acceptors made accessible to *S. oneidensis* by EET do not produce a gradient, and *S. oneidensis* still exhibits a chemotactic response near their surface (Bencharit & Ward, 2005; Harris *et al.*, 2010). Thus, a new process related to chemotaxis toward anaerobic, insoluble electron acceptors has been proposed: electrolocation (Harris *et al.*, 2010; Starwalt-Lee *et al.*, 2021).

Electrolocation is known to require both a functional chemotaxis pathway and a functional EET pathway (Harris *et al.*, 2010; Harris *et al.*, 2012), but the link between chemotaxis and EET has remained indefinite. A growing body of literature has implicated redox-active flavins such as FMN as the critical component to the electrolocation phenotype. *S. oneidensis* cells secrete flavins in the form of FAD which is cleaved into FMN and AMP in the periplasm (Covington *et al.*, 2010). The FMN then diffuses out of the cell and acts as a reversible electron shuttle, capable of being reduced by the outer membrane EET protein MtrC and subsequently oxidized by a nearby electron acceptor (Brutinel & Gralnick, 2011). It can then diffuse back to the cell in its oxidized form to be reduced once again. As *S. oneidensis* cells release flavins into their surroundings, it is possible that a gradient of reduced to oxidized flavins forms, where a higher concentration of reduced flavins occurs within the cell's vicinity, and a higher concentration of oxidized flavins occurs near a more distant, insoluble electron acceptor such as an electrode. In this way, cells may be able to move up a gradient of oxidized flavins in order to reach the IEA, thus using chemotaxis to locate the IEA and EET to interact with the redox-active flavins.

Both microfluidic experiments and swim plate experiments have been performed to show that flavins are indeed a chemoattractant for *S. oneidensis* (Kim *et al.*, 2016; R. Li *et al.*, 2012), and additional experiments have demonstrated that the chemotactic behavior around an electrode occurs at a potential of −0.2 V vs SHE, the midpoint potential of flavins (Oram & Jeuken, 2019). Also, there is evidence that some chemotactic signals may not provide a direct growth benefit but may signal that food is nearby (Tohidifar *et al.*, 2020). Thus, given the chemoattractant nature of flavins, studies have suggested that the cells not only use flavins as an electron shuttle but also for mediating chemotaxis toward IEAs (R. Li *et al.*, 2012). However, the experiments were unable to claim that oxidized flavins were the specific chemoattractant (J. Li *et al.*, 2010), and more work was needed to prove that oxidized flavins enable chemotaxis toward IEAs.

The goal of this thesis was to establish an experimental framework that would tease apart the nuances of electrolocation and test whether oxidized flavins facilitate *S. oneidensis* chemotaxis toward a poised electrode. By using a custom microscope slide equipped with ITO electrodes and applying potential to the system, both a flavin redox gradient and cell motility trends were able to be visualized. Though the experiments were only performed once, the responses of WT, Δ*cheA-3*, and ΔEET strains to the poised electrode were broadly consistent with prior literature on flavin-mediated taxis in shewanellae (Harris *et al.*, 2010; R. Li *et al.*, 2012). WT cells responded strongly to oxidizing electrode potentials, showing both increased swim speeds and congregation. The Δ*cheA-3* cells, which lacked the ability to reverse swimming direction, did not congregate but displayed localized increases in swim speed at the working electrode. Their increase in swim speed at the poised electrode indicated their ability to respire using the electrode and gain energy, but it did not denote the phenotype of electrolocation. The ΔEET cells had significant metabolic limitations and showed neither congregation nor increased motility, solidifying the connection between energy availability and electrolocation. These findings highlight the interplay between chemotaxis machinery, electron transfer capability, and metabolic state in governing motility responses toward poised electrodes. They also establish the validity of the experimental setup and provide a foundation for future experiments with increased repetitions, standardized media components, and precise strain selection.

Future Directions

The work in this thesis opens the door to live-cell imaging of motile bacteria in response to a poised electrode. As such, there are multiple directions with which to take future experiments. First, testing shewanellae in the presence of nanomolar concentrations of flavins (Marsili *et al.*, 2008) could provide a more accurate representation of what chemotaxis looks like under physiologically relevant flavin concentrations. Second, a control experiment with limited flavins in the environment could be implemented, where cultures are washed at low spin speeds (Bennett *et al.*, 2016) in flavin-free media before being tested in the electrochemical system. To further remove flavins from experimental conditions, a mutant lacking the gene responsible for FAD export, *bfe*, could be used to inhibit flavins from diffusing out of the cell and into the environment (Kotloski *et al.*, 2013). In combination with washing steps, the *S. oneidensis* Δ*bfe* strain would have virtually no interaction with flavins, and congregation at the electrode would be expected to be nearly abolished. However, experimental parameters may have to be adjusted with the *S. oneidensis* Δ*bfe* strain, since lacking Bfe, it also lacks periplasmic FAD that is used as a cofactor for the fumarate reductase, FccA (Kees *et al.*, 2019).

Another strain that would be interesting to test in the electrochemical system is *S. denitrificans*. The strain does not have the capacity to reduce insoluble iron, but it still excretes flavins (Coursolle *et al.*, 2010). If oxidized flavins serve to aid shewanellae navigation toward insoluble electron acceptors, *S. denitrificans* might still have the redox-sensing machinery necessary for locating and navigating insoluble electron acceptors, and its motility patterns might change in relation to a poised electrode.

Little is known about the redox-sensing mechanisms of *S. oneidensis*, and more studies correlating MCP activity to substrate are needed. Making systematic deletions of MCP genes from the *S. oneidensis* genome and measuring the difference in response to the poised electrode would be critical for understanding what molecular interactions are responsible for the phenotype of electrolocation. Initial experiments could begin with deleting genes responsible for MCPs such as SO_2240 that have been shown to be necessary for energy taxis to fumarate (Harris *et al.*, 2012, 2018).

Furthermore, electrolocation depends on a functional EET pathway (Harris *et al.*, 2010), and certain cytochromes offer substrate-specific activity (Coursolle & Gralnick, 2010). The specific reason that cytochromes are required for electrolocation remains unknown. Mutants lacking *cymA*, and mutants lacking *mtrBC* in addition to *omcA* have been tested and have proven

deficient in electrolocation (Harris *et al*., 2012), but more experiments are needed to isolate which cytochromes are most important for electrolocation and why.

REFERENCES

Baraquet, C., Théraulaz, L., Iobbi-Nivol, C., Méjean, V., & Jourlin-Castelli, C. (2009). Unexpected chemoreceptors mediate energy taxis towards electron acceptors in *Shewanella oneidensis*. *Molecular Microbiology*, 73(2), 278–290. https://doi.org/10.1111/j.1365-2958.2009.06770.x

Baron, D., LaBelle, E., Coursolle, D., Gralnick, J. A., & Bond, D. R. (2009). Electrochemical Measurement of Electron Transfer Kinetics by *Shewanella oneidensis* MR-1. *Journal of Biological Chemistry*, 284(42), 28865–28873. https://doi.org/10.1074/jbc.m109.043455

Bencharit, S., & Ward, M. J. (2005). Chemotactic Responses to Metals and Anaerobic Electron Acceptors in *Shewanella oneidensis* MR-1. *Journal of Bacteriology*, 187(14), 5049–5053. https://doi.org/10.1128/jb.187.14.5049-5053.2005

Berg, H. C. (1975). Chemotaxis in Bacteria. *Annual Review of Biophysics and Bioengineering*, 4(1), 119–136. https://doi.org/10.1146/annurev.bb.04.060175.001003

Berg, H. C., & Anderson, R. A. (1973). Bacteria Swim by Rotating their Flagellar Filaments. *Nature* (London), 245(5425), 380–382. https://doi.org/10.1038/245380a0

Bretschger, O., Obraztsova, A., Sturm, C. A., Chang, I. S., Gorby, Y. A., Reed, S. B., Culley, D. E., Reardon, C. L., Barua, S., Romine, M. F., Zhou, J., Beliaev, A. S., Bouhenni, R., Saffarini, D., Mansfeld, F., Kim, B.-H., Fredrickson, J. K., & Nealson, K. H. (2007). Current Production and Metal Oxide Reduction by *Shewanella oneidensis* MR-1 Wild Type and Mutants. *Applied and Environmental Microbiology*, 73(21), 7003–7012. https://doi.org/10.1128/aem.01087-07

Brutinel, E. D., & Gralnick, J. A. (2012). Shuttling happens: Soluble flavin mediators of extracellular electron transfer in *Shewanella*. *Applied Microbiology and Biotechnology*, 93(1), 41–48. https://doi.org/10.1007/s00253-011-3653-0

Clarke, T. A., Edwards, M. J., Gates, A. J., Hall, A., White, G. F., Bradley, J., Reardon, C. L., Shi, L., Beliaev, A. S., Marshall, M. J., Wang, Z., Watmough, N. J., Fredrickson, J. K., Zachara, J. M., Butt, J. N., & Richardson, D. J. (2011). Structure of a bacterial cell surface decaheme electron conduit. *Proceedings of the National Academy of Sciences*, 108(23), 9384–9389. https://doi.org/10.1073/pnas.1017200108

Coursolle, D., Baron, D. B., Bond, D. R., & Gralnick, J. A. (2010). The Mtr Respiratory Pathway Is Essential for Reducing Flavins and Electrodes in *Shewanella oneidensis*. *Journal of Bacteriology*, 192(2), 467–474. https://doi.org/10.1128/jb.00925-09

Coursolle, D., & Gralnick, J. A. (2010). Modularity of the Mtr respiratory pathway of *Shewanella oneidensis* strain MR-1. *Molecular Microbiology*, 77(4), 995–1008. https://doi.org/10.1111/j.1365-2958.2010.07266.x

Covington, E. D., Gelbmann, C. B., Kotloski, N. J., & Gralnick, J. A. (2010). An essential role for UshA in processing of extracellular flavin electron shuttles by *Shewanella oneidensis*. *Molecular Microbiology*, 78(2), 519–532. https://doi.org/10.1111/j.1365-2958.2010.07353.x

Ecophysiology of the Genus *Shewanella*. (2006). In K. H. Nealson & J. Scott, The Prokaryotes (pp. 1133–1151). Springer New York. https://doi.org/10.1007/0-387-30746-x_45

Edwards, M. J., White, G. F., Butt, J. N., Richardson, D. J., & Clarke, T. A. (2020). The Crystal Structure of a Biological Insulated Transmembrane Molecular Wire. *Cell*, 181(3), 665-673.e10. https://doi.org/10.1016/j.cell.2020.03.032

Fonseca, B. M., Paquete, C. M., Neto, S. E., Pacheco, I., Soares, C. M., & Louro, R. O. (2013). Mind the gap: Cytochrome interactions reveal electron pathways across the periplasm of *Shewanella oneidensis* MR-1. *Biochemical Journal*, 449(1), 101–108. https://doi.org/10.1042/BJ20121467

Fredrickson, J. K., Romine, M. F., Beliaev, A. S., Auchtung, J. M., Driscoll, M. E., Gardner, T. S., Nealson, K. H., Osterman, A. L., Pinchuk, G., Reed, J. L., Rodionov, D. A., Rodrigues, J. L. M., Saffarini, D. A., Serres, M. H., Spormann, A. M., Zhulin, I. B., & Tiedje, J. M. (2008). Towards environmental systems biology of *Shewanella*. *Nature Reviews Microbiology*, 6(8), 592–603. https://doi.org/10.1038/nrmicro1947

Gorby, Y. A., Yanina, S., McLean, J. S., Rosso, K. M., Moyles, D., Dohnalkova, A., Beveridge, T. J., Chang, I. S., Kim, B. H., Kim, K. S., Culley, D. E., Reed, S. B., Romine, M. F., Saffarini, D. A., Hill, E. A., Shi, L., Elias, D. A., Kennedy, D. W., Pinchuk, G., … Fredrickson, J. K. (2006). Electrically conductive bacterial nanowires produced by *Shewanella oneidensis* strain MR-1 and other microorganisms. *Proceedings of the National Academy of Sciences*, 103(30), 11358–11363. https://doi.org/10.1073/pnas.0604517103

Gralnick, J. A., & Bond, D. R. (2023). Electron Transfer Beyond the Outer Membrane: Putting Electrons to Rest. *Annual Review of Microbiology*, 77(1), 517–539. https://doi.org/10.1146/annurev-micro-032221-023725

Gralnick, J. A., & Newman, D. K. (2007). Extracellular respiration. *Molecular Microbiology*, 65(1), 1–11. https://doi.org/10.1111/j.1365-2958.2007.05778.x

Harris, H. W., El-Naggar, M. Y., Bretschger, O., Ward, M. J., Romine, M. F., Obraztsova, A. Y., & Nealson, K. H. (2010). Electrokinesis is a microbial behavior that requires extracellular electron transport. *Proceedings of the National Academy of Sciences*, 107(1), 326–331. https://doi.org/10.1073/pnas.0907468107

Harris, H. W., El-Naggar, M. Y., & Nealson, K. H. (2012). *Shewanella oneidensis* MR-1 chemotaxis proteins and electron-transport chain components essential for congregation near insoluble electron acceptors. *Biochemical Society Transactions*, 40(6), 1167–1177. https://doi.org/10.1042/bst20120232

Harris, H. W., Sánchez-Andrea, I., McLean, J. S., Salas, E. C., Tran, W., El-Naggar, M. Y., & Nealson, K. H. (2018). Redox Sensing within the Genus *Shewanella*. *Frontiers in Microbiology*, 8. https://doi.org/10.3389/fmicb.2017.02568

Hartshorne, R. S., Reardon, C. L., Ross, D., Nuester, J., Clarke, T. A., Gates, A. J., Mills, P. C., Fredrickson, J. K., Zachara, J. M., Shi, L., Beliaev, A. S., Marshall, M. J., Tien, M., Brantley, S., Butt, J. N., & Richardson, D. J. (2009). Characterization of an electron conduit between bacteria

and the extracellular environment. *Proceedings of the National Academy of Sciences*, 106(52), 22169–22174. https://doi.org/10.1073/pnas.0900086106

Hau, H. H., Gilbert, A., Coursolle, D., & Gralnick, J. A. (2008). Mechanism and Consequences of Anaerobic Respiration of Cobalt by *Shewanella oneidensis* Strain MR-1. *Applied and Environmental Microbiology*, 74(22), 6880–6886. https://doi.org/10.1128/AEM.00840-08

Hau, H. H., & Gralnick, J. A. (2007). Ecology and Biotechnology of the Genus *Shewanella*. *Annual Review of Microbiology*, 61(1), 237–258. https://doi.org/10.1146/annurev.micro.61.080706.093257

Heidelberg, J. F., Paulsen, I. T., Nelson, K. E., Gaidos, E. J., Nelson, W. C., Read, T. D., Eisen, J. A., Seshadri, R., Ward, N., Methe, B., Clayton, R. A., Meyer, T., Tsapin, A., Scott, J., Beanan, M., Brinkac, L., Daugherty, S., DeBoy, R. T., Dodson, R. J., … Fraser, C. M. (2002). Genome sequence of the dissimilatory metal ion–reducing bacterium *Shewanella oneidensis*. *Nature Biotechnology*, 20(11), 1118–1123. https://doi.org/10.1038/nbt749

Kappler, A., Bryce, C., Mansor, M., Lueder, U., Byrne, J. M., & Swanner, E. D. (2021). An evolving view on biogeochemical cycling of iron. *Nature Reviews Microbiology*, 19(6), 360–374. https://doi.org/10.1038/s41579-020-00502-7

Keegstra, J. M., Carrara, F., & Stocker, R. (2022). The ecological roles of bacterial chemotaxis. *Nature Reviews Microbiology*, 20(8), 491–504. https://doi.org/10.1038/s41579-022-00709-w

Kees, E. D., Pendleton, A. R., Paquete, C. M., Arriola, M. B., Kane, A. L., Kotloski, N. J., Intile, P. J., & Gralnick, J. A. (2019). Secreted Flavin Cofactors for Anaerobic Respiration of Fumarate and Urocanate by *Shewanella oneidensis*: Cost and Role. *Applied and Environmental Microbiology*, 85(16). https://doi.org/10.1128/aem.00852-19

Kim, B. J., Chu, I., Jusuf, S., Kuo, T., TerAvest, M. A., Angenent, L. T., & Wu, M. (2016). Oxygen Tension and Riboflavin Gradients Cooperatively Regulate the Migration of *Shewanella oneidensis* MR-1 Revealed by a Hydrogel-Based Microfluidic Device. *Frontiers in Microbiology*, 7. https://doi.org/10.3389/fmicb.2016.01438

Kotloski, N. J., & Gralnick, J. A. (2013). Flavin Electron Shuttles Dominate Extracellular Electron Transfer by *Shewanella oneidensis*. *mBio*, 4(1), e00553-12. https://doi.org/10.1128/mBio.00553-12

Li, J., Go, A. C., Ward, M. J., & Ottemann, K. M. (2010). The chemical-in-plug bacterial chemotaxis assay is prone to false positive responses. *BMC Research Notes*, 3(1), 77. https://doi.org/10.1186/1756-0500-3-77

Li, J., Romine, M. F., & Ward, M. J. (2007). Identification and analysis of a highly conserved chemotaxis gene cluster in *Shewanella* species. *FEMS Microbiology Letters*, 273(2), 180–186. https://doi.org/10.1111/j.1574-6968.2007.00810.x

Li, R., Tiedje, J. M., Chiu, C., & Worden, R. M. (2012). Soluble Electron Shuttles Can Mediate Energy Taxis toward Insoluble Electron Acceptors. *Environmental Science & Technology*, 46(5), 2813–2820. https://doi.org/10.1021/es204302w

Li, Y., Liu, K., Mao, R., Liu, B., Cheng, L., & Shi, X. (2022). Unveiling the chemotactic response and mechanism of *Shewanella oneidensis* MR-1 to nitrobenzene. *Journal of Hazardous Materials*, 431, 128629. https://doi.org/10.1016/j.jhazmat.2022.128629

MacDonell, M. T., & Colwell, R. R. (1985). Phylogeny of the Vibrionaceae, and Recommendation for Two New Genera, *Listonella* and *Shewanella*. *Systematic and Applied Microbiology*, 6(2), 171–182. https://doi.org/10.1016/S0723-2020(85)80051-5

Marshall, M. J., Beliaev, A. S., Dohnalkova, A. C., Kennedy, D. W., Shi, L., Wang, Z., Boyanov, M. I., Lai, B., Kemner, K. M., McLean, J. S., Reed, S. B., Culley, D. E., Bailey, V. L., Simonson, C. J., Saffarini, D. A., Romine, M. F., Zachara, J. M., & Fredrickson, J. K. (2006). *c*-Type Cytochrome-Dependent Formation of U(IV) Nanoparticles by *Shewanella oneidensis*. *PLoS Biology*, 4(8), e268. https://doi.org/10.1371/journal.pbio.0040268

Marsili, E., Baron, D. B., Shikhare, I. D., Coursolle, D., Gralnick, J. A., & Bond, D. R. (2008). *Shewanella* secretes flavins that mediate extracellular electron transfer. *Proceedings of the National Academy of Sciences*, 105(10), 3968–3973. https://doi.org/10.1073/pnas.0710525105

Murphy, J. N., & Saltikov, C. W. (2007). The *cymA* Gene, Encoding a Tetraheme *c*-Type Cytochrome, Is Required for Arsenate Respiration in *Shewanella* Species. *Journal of Bacteriology*, 189(6), 2283–2290. https://doi.org/10.1128/JB.01698-06

Myers, C. R., & Myers, J. M. (1997). Cloning and sequence of *cymA*, a gene encoding a tetraheme cytochrome *c* required for reduction of iron(III), fumarate, and nitrate by *Shewanella putrefaciens* MR-1. *Journal of Bacteriology*, 179(4), 1143–1152. https://doi.org/10.1128/jb.179.4.1143-1152.1997

Myers, C. R., & Nealson, K. H. (1988). Bacterial Manganese Reduction and Growth with Manganese Oxide as the Sole Electron Acceptor. *Science (American Association for the Advancement of Science)*, 240(4857), 1319–1321. https://doi.org/10.1126/science.240.4857.1319

Myers, C. R., & Nealson, K. H. (1990). Respiration-linked proton translocation coupled to anaerobic reduction of manganese(IV) and iron(III) in *Shewanella putrefaciens* MR-1. *Journal of Bacteriology*, 172(11), 6232–6238. https://doi.org/10.1128/jb.172.11.6232-6238.1990

Nealson, K. H. (2017). Bioelectricity (electromicrobiology) and sustainability. *Microbial Biotechnology*, 10(5), 1114–1119. https://doi.org/10.1111/1751-7915.12834

Nealson, K. H., Moser, D. P., & Saffarini, D. A. (1995). Anaerobic electron acceptor chemotaxis in *Shewanella putrefaciens*. *Applied and Environmental Microbiology*, 61(4), 1551–1554. https://doi.org/10.1128/aem.61.4.1551-1554.1995

Okamoto, A., Kalathil, S., Deng, X., Hashimoto, K., Nakamura, R., & Nealson, K. H. (2014). Cell-secreted Flavins Bound to Membrane Cytochromes Dictate Electron Transfer Reactions to Surfaces with Diverse Charge and pH. *Scientific Reports*, 4(1), 5628. https://doi.org/10.1038/srep05628

Oram, J., & Jeuken, L. J. C. (2019). Tactic Response of *Shewanella oneidensis* MR-1 toward Insoluble Electron Acceptors. *mBio*, 10(1), e02490-18. https://doi.org/10.1128/mBio.02490-18

Paquete, C. M., Fonseca, B. M., Cruz, D. R., Pereira, T. M., Pacheco, I., Soares, C. M., & Louro, R. O. (2014). Exploring the molecular mechanisms of electron shuttling across the microbe/metal space. *Frontiers in Microbiology*, 5. https://doi.org/10.3389/fmicb.2014.00318

Pitts, K. E., Dobbin, P. S., Reyes-Ramirez, F., Thomson, A. J., Richardson, D. J., & Seward, H. E. (2003). Characterization of the *Shewanella oneidensis* MR-1 Decaheme Cytochrome MtrA. *Journal of Biological Chemistry*, 278(30), 27758–27765. https://doi.org/10.1074/jbc.M302582200

Saffarini, D. A., Blumerman, S. L., & Mansoorabadi, K. J. (2002). Role of Menaquinones in Fe(III) Reduction by Membrane Fractions of *Shewanella putrefaciens*. *Journal of Bacteriology*, 184(3), 846–848. https://doi.org/10.1128/JB.184.3.846-848.2002

Saltikov, C. W., & Newman, D. K. (2003). Genetic identification of a respiratory arsenate reductase. *Proceedings of the National Academy of Sciences*, 100(19), 10983–10988. https://doi.org/10.1073/pnas.1834303100

Schuetz, B., Schicklberger, M., Kuermann, J., Spormann, A. M., & Gescher, J. (2009). Periplasmic Electron Transfer via the *c*-Type Cytochromes MtrA and FccA of *Shewanella oneidensis* MR-1. *Applied and Environmental Microbiology*, 75(24), 7789–7796. https://doi.org/10.1128/AEM.01834-09

Schwalb, C., Chapman, S. K., & Reid, G. A. (2002). The membrane-bound tetrahaem *c*-type cytochrome CymA interacts directly with the soluble fumarate reductase in *Shewanella*. *Biochemical Society Transactions*, 30(4), 658–662. https://doi.org/10.1042/bst0300658

Shi, L., Squier, T. C., Zachara, J. M., & Fredrickson, J. K. (2007). Respiration of metal (hydr)oxides by *Shewanella* and *Geobacter*: A key role for multihaem *c*-type cytochromes. *Molecular Microbiology*, 65(1), 12–20. https://doi.org/10.1111/j.1365-2958.2007.05783.x

Snell-Rood, E. (2016). Bring biologists into biomimetics. *Nature* (London), 529(7586), 277. https://doi.org/10.1038/529277a

Starwalt-Lee, R., El-Naggar, M. Y., Bond, D. R., & Gralnick, J. A. (2021). Electrolocation? The evidence for redox-mediated taxis in *Shewanella oneidensis*. *Molecular Microbiology*, 115(6), 1069–1079. https://doi.org/10.1111/mmi.14647

Stocker, R. (2011). Reverse and flick: Hybrid locomotion in bacteria. *Proceedings of the National Academy of Sciences*, 108(7), 2635–2636. https://doi.org/10.1073/pnas.1019199108

Stricker, L., Guido, I., Breithaupt, T., Mazza, M. G., & Vollmer, J. (2020). Hybrid sideways/longitudinal swimming in the monoflagellate *Shewanella oneidensis*: From aerotactic band to biofilm. *Journal of The Royal Society Interface*, 17(171), 20200559. https://doi.org/10.1098/rsif.2020.0559

Thormann, K. M., Beta, C., & Kühn, M. J. (2022). Wrapped Up: The Motility of Polarly Flagellated Bacteria. *Annual Review of Microbiology*, 76(1), 349–367. https://doi.org/10.1146/annurev-micro-041122-101032

Tohidifar, P., Bodhankar, G. A., Pei, S., Cassidy, C. K., Walukiewicz, H. E., Ordal, G. W., Stansfeld, P. J., & Rao, C. V. (2020). The Unconventional Cytoplasmic Sensing Mechanism for Ethanol Chemotaxis in *Bacillus subtilis*. *mBio*, 11(5), e02177-20. https://doi.org/10.1128/mBio.02177-20

Venkateswaran, K., Moser, D. P., Dollhopf, M. E., Lies, D. P., Saffarini, D. A., MacGregor, B. J., Ringelberg, D. B., White, D. C., Nishijima, M., Sano, H., Burghardt, J., Stackebrandt, E., & Nealson, K. H. (1999). Polyphasic taxonomy of the genus *Shewanella* and description of *Shewanella oneidensis* sp. nov. *International Journal of Systematic and Evolutionary Microbiology*, 49(2), 705–724. https://doi.org/10.1099/00207713-49-2-705

Vinnichenko, G., Jarrett, A. J. M., Hope, J. M., & Brocks, J. J. (2020). Discovery of the oldest known biomarkers provides evidence for phototrophic bacteria in the 1.73 Ga Wollogorang Formation, Australia. *Geobiology*, 18(5), 544–559. https://doi.org/10.1111/gbi.12390

Von Canstein, H., Ogawa, J., Shimizu, S., & Lloyd, J. R. (2008). Secretion of Flavins by *Shewanella* Species and Their Role in Extracellular Electron Transfer. *Applied and Environmental Microbiology*, 74(3), 615–623. https://doi.org/10.1128/AEM.01387-07

APPENDIX A

A1. Thresholding Function in Python Code Led to Graphing Abnormality

Parameters of the thresholding function which was used in the Python code to calculate pixel intensities included the edge of the electrode erroneously (Figure A1). Future experiments will adjust the calculations accordingly.

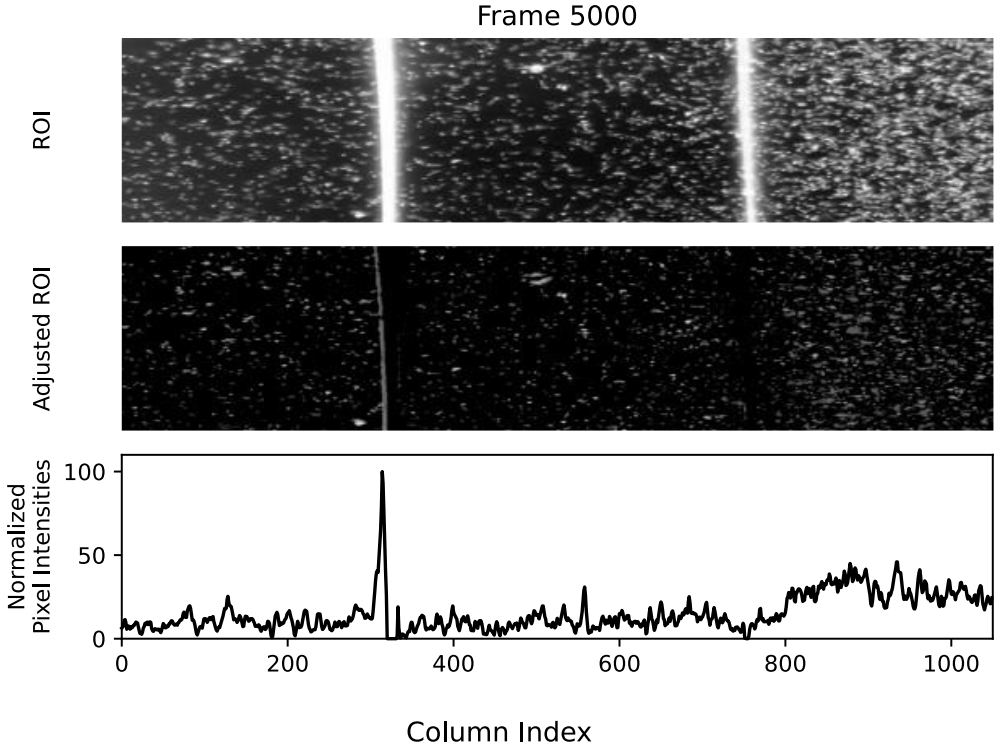

Figure A1: Frame 5000 of WT *S. oneidensis* video recording, with the working electrode on the left. A thresholding error in the code included the edge of the working electrode in the adjusted ROI frame, resulting in a peak near column index 320 that was not attributed to cell density.

A2. Full Python Code

```
import os
import cv2
import matplotlib.pyplot as plt
import numpy as np
from scipy.ndimage import median_filter

DATE = '20250809'
FILE_LOCATION = r"C:\Users" # insert file path here

video_path = os.path.join(FILE_LOCATION, 'VIDEO NAME') # insert the name of the video as a string
```

```
video_for_analysis = video_path
cap = cv2.VideoCapture(video_for_analysis) # load video file

MAX_INTENSITY = 0 # begins the maximum intensity count at 0
frame_number = 0  # starts the frame count at 0
frame_limit = 16000 # number of frames that will be read before breaking out of while loop
# can also do the full length of the video using: int(cap.get(cv2.CAP_PROP_FRAME_COUNT))
accumulator = None # placeholder used to accumulate regions of interest

grouping = 500  # variable used to determine what frames are selected.
# If grouping = 10, 1 frame would be collected every 10 frames
results = []
hist_sums = []  # for collecting sums of heights for every frame
hist_sums_select = []  # for collecting sums from select frames
last_roi = None

# define dimensions of the ROI:
y1 = 500
y2 = 1100
x1 = 400
x2 = 1450

FIG_FILEENDING = '.svg' # will save file in the format recorded here.
VIDEO_NAME = os.path.splitext(os.path.basename(video_path))[0]
WORKING_FOLDER = os.path.join(FILE_LOCATION, DATE, VIDEO_NAME)
os.makedirs(WORKING_FOLDER, exist_ok=True) # make a folder to store data.
# First folder will have the date, nested folder will have the video name as the title)

fps = cap.get(cv2.CAP_PROP_FPS) # retreive the video's fps
width  = int(cap.get(cv2.CAP_PROP_FRAME_WIDTH))
height = int(cap.get(cv2.CAP_PROP_FRAME_HEIGHT))
print(width)
print(height)

# cap is the video object from cv2.VideoCapture(video_for_analysis)
# cap.isOpened() returns True if the video file was successfully opened.
while cap.isOpened():
   # read frames
   success, frame = cap.read()
   # success is a boolean returning true or false depending on whether the frame was successfully
read
   # frame is the variable storing actual image data

   if not success:
      print("Video has ended.")
      break

   if frame_number > frame_limit:
      print("Reached frame limit.")
      break
```

```
    gray_image_start = cv2.cvtColor(frame, cv2.COLOR_BGR2GRAY)
    # roi = gray_image_start[200:800, 400:1600]
    roi = gray_image_start[y1:y2, x1:x2]
    # roi is the region of interest for analysis. It is a NumPy array of pixel intensities.
    # roi is a matrix of values from 0 to 255 (one per pixel) bc I am working in grayscale.

    # To examine the roi captured from the last video frame, use:
    # if frame_number == (frame_limit - 1):
    #     last_roi = roi.copy()

    # accumulator collects the NumPy array of pixel intensities and stores them as a float number
    if accumulator is None:
        accumulator = roi.astype("float")
    else:
        accumulator += roi

    frame_number += 1 # advance the frame count by 1

    background = (accumulator / frame_number).astype("uint8")
    # accounts for non-motile objects bc it assumes that non-moving objects stay the same and
moving objects vary
    # across frames, thus becoming blurred out or dimmed in the average

    foreground = cv2.absdiff(roi, background)
    # isolates movement by showing how different the current frame is from the expected
background

    _, cleaned = cv2.threshold(foreground, 50, 255,
                               cv2.THRESH_TOZERO)  # Apply threshold to remove small differences
such as noise

    # Sum along the x-axis (columns); used to make histogram; includes evey frame < frame_limit
    collapse = cleaned.sum(axis=0)  # axis=0 in .sum() collapses rows => summing brightness
across height.
    # produces an array where each element is the sum of pixel intensities
    # for that column in your ROI for the current frame

    frame_max = max(collapse)
    if frame_number % grouping == 0:
        MAX_INTENSITY = max(MAX_INTENSITY, frame_max)
        # want the maximum intensity within each frame compared against each frame

    if frame_number % grouping == 0:
        #print(f"Frame#: {frame_number}")
        collapse_select = cleaned.sum(
            axis=0)
        # MAX_INTENSITY = max([max(collapse_select), MAX_INTENSITY])
        #if frame_number == 5 or frame_number % (grouping * 5) == 0:
            #MAX_INTENSITY = max([max(collapse_select), MAX_INTENSITY])
```

```
print(f"Max intensity: {MAX_INTENSITY}") # sanity check
cap.release()

# Reset and examine the video data again to calculate the max intensity of all frames and plot the
histograms
frame_number = 0
accumulator = None

cap = cv2.VideoCapture(video_for_analysis)
while cap.isOpened():
    # read frames
    success, frame = cap.read()
    # success is a boolean returning true or false depending on whether the frame was successfully
read
    # frame is the variable storing actual image data

    if not success:
        print("Video has ended.")
        break

    if frame_number > frame_limit:
        print("Reached frame limit.")
        break

    gray_image_start = cv2.cvtColor(frame, cv2.COLOR_BGR2GRAY)
    # roi = gray_image_start[200:800, 400:1600]
    roi = gray_image_start[y1:y2, x1:x2]
    # roi is the region of interest for analysis.
    # It is a NumPy array of pixel intensities. roi is a matrix of values from 0 to 255 (one per pixel)
    # bc I am working in grayscale.

    # if frame_number == (frame_limit - 1):
    #     last_roi = roi.copy()

    if accumulator is None:
        accumulator = roi.astype("float")
    else:
        accumulator += roi
    background = (accumulator / frame_number).astype("uint8")

    frame_number += 1

    # accounts for non-motile objects bc it assumes that non-moving objects stay the same and
moving objects vary
    # across frames, thus becoming blurred out or dimmed in the average

    foreground = cv2.absdiff(
        roi,
        background,
```

```
    )  # isolates movement by showing how different the current frame is from the expected
background

    _, cleaned = cv2.threshold(foreground, 50, 255,
                               cv2.THRESH_TOZERO)  # Apply threshold to remove small differences
such as noise

    # Sum across rows to make histogram; includes evey frame < frame_limit
    collapse = cleaned.sum(axis=0)  # axis=0 in .sum() collapses rows => summing brightness
across height.
    # collapse = foreground.sum(axis=0) # axis=0 in .sum() collapses rows => summing brightness
across height.
    hist_sums.append(collapse)

    if frame_number % grouping == 0:
        # print(f"Frame number: {frame_number} - plotting")
        collapse_select = cleaned.sum(axis=0)
        # axis=0 in .sum() collapses rows => summing brightness across height depending on
grouping variable

        hist_sums_select.append(
            (frame_number, collapse_select))  # collects selected sums and makes them a tuple
(frame, selected data)

        normalized = collapse_select * (100 / MAX_INTENSITY)
        if MAX_INTENSITY > 0 and (frame_number == 500 or (frame_number % (grouping * 5)
== 0)):
            fig, ax = plt.subplots(
                3, 1,
                height_ratios=[1, 1, 1]
            )
            ax[0].imshow(roi, cmap='gray', aspect="auto")
            ax[0].set_title(f"Frame {frame_number}")
            ax[0].set_ylabel('ROI')
            ax[0].tick_params(left=False, bottom=False, labelleft=False, labelbottom=False)
            for spine in ax[0].spines.values():
                spine.set_visible(False)

            ax[1].imshow(cleaned, cmap='gray', aspect="auto")
            #ax[1].set_title(f"Frame {frame_number}")
            ax[1].set_ylabel('Adjusted ROI')
            ax[1].tick_params(left=False, bottom=False, labelleft=False, labelbottom=False)
            for spine in ax[1].spines.values():
                spine.set_visible(False)

            ax[2].set_xlim([0, x2 - x1])
            ax[2].set_ylim([0, 100 * 1.1])
            ax[2].set_ylabel('Normalized\nPixel Intensities')
            ax[2].plot(
                normalized,
```

```
            # label=f'Frame {frame_idx}',
            color='black',
        )
        fig.supxlabel('Column Index')
        fig.align_ylabels(ax)
        fig.tight_layout()
        # plt.show()
        plt.savefig(
            os.path.join(WORKING_FOLDER,
f"{VIDEO_NAME}_histogram_{frame_number}{FIG_FILEENDING}")
        )
        plt.close()
    #else:
        #print(f"Frame number: {frame_number}")
cap.release()

print('roi numpy array:', roi[0])
#print('background numpy array:', background[0])

# Use if visualizing the ROI of the last frame is desired
# if last_roi is not None:
#     plt.imshow(last_roi, cmap='gray')
#     plt.title(f"Frame {frame_limit - 1}")
#     plt.axis('on')
#     #plt.show()
#print(last_roi) # sanity check

plt.figure(figsize=(12, 7))

c_results = hist_sums_select.copy()  # use this line if grouping variable was sufficient for
collecting frames you want
# c_results = list(enumerate(hist_sums_select))[::100] # use this line if grouping variable is low,
# and you don't want to re-run the video, but you want to select every nth element

colors = plt.cm.plasma(np.linspace(0, 1, len(c_results)))
for i, (frame_idx, res) in enumerate(c_results):
    #print(f"Plotting frame {frame_idx}")  # Debug line
    # print(f"Type: {type(res)}, shape: {np.shape(res)}")
    current_result = median_filter(res, 20)
    normalized_current_result = (current_result / MAX_INTENSITY) * 100
    print('NCR',normalized_current_result[0])
    plt.plot(
        normalized_current_result,
        label=f'Frame {frame_idx}',
        color=colors[i],
    )
plt.title("Motion Histograms Over Time")
plt.xlabel("Column Index")
plt.ylabel("Normalized Pixel Intensities")
plt.xlim([0, x2 - x1])
```

```
plt.ylim([0, 100 * 1.1]) # leave room to be above the maximum by multiplying upper limit by 1.1
plt.legend(
    bbox_to_anchor=(1.01, 1),  # x = 1.05 puts it outside the plot
    loc='upper left',  # anchors the legend's upper left corner
    borderaxespad=0.,  # reduce padding between plot and legend
    fontsize=8.5        # can also say 'small'
    #ncols = 2          # make the legend go into two columns
)
plt.tight_layout()
# plt.show()
plt.savefig(
    os.path.join(WORKING_FOLDER,
f"{VIDEO_NAME}_histogram_collated_{frame_number}{FIG_FILEENDING}"),
    dpi=300, # figure-grade resolution
    # bbox_inches='tight',
    transparent=True,
)
```

A3. Information Regarding Supplementary Movies

Table A: Description of movies including the approximate times at which conditions occur

Movie Name	Movie Content	Location of Poised Electrode	~Time Oxidizing Conditions Begin (min:sec)	~Time Oxidizing Conditions End (min:sec)
Movie 1	FMN color change	NA	NA	NA
Movie 2	*S. oneidensis* MR-1	Right electrode	00:18	20:21
Movie 3	*S. oneidensis* MR-1	Left electrode	00:25	15:28
Movie 4	*S. oneidensis* Δ*cheA-3*	Right electrode	01:17	16:20
Movie 5	*S. oneidensis* Δ*cheA-3*	Left electrode	00:30	15:33
Movie 6	*S. oneidensis* ΔEET	Right electrode	03:00	18:03
Movie 7	*S. oneidensis* ΔEET	Left electrode	00:30	15:33